We thank the reviewers for their thoughtful comments, and address each point below. We note changes that have been made to the manuscript. Original reviewer comments are in **black** and our responses in **blue**. New text added is *italicized*.

Response to Reviewer #1

Overall impression
The manuscript 'Measurement and modeling of the multi-wavelength optical properties of uncoated flame-generated soot' by Forestieri et al. presents a detailed analysis of laboratory studies of black carbon particles to rationalize a more appropriate (Rayleigh- Debye-Gans approximation) that uses a constant mass absorption coefficient that is size independent, but wavelength specific treatment of uncoated BC particles within climate models. The authors present a clear question, clearly answer it and the findings fall within the scope of ACP. The manuscript is technical, well-written, and provides a clear connection between laboratory experiments and conclusions. I have no major comments and recommend this manuscript for publication.

We thank the reviewer for the thoughtful review.

Significant time is devoted to placing these measurements in context, but there is frequently no suggestion as to why these measurements are different – when they are that is. I suggest providing the reader some guidance as to the authors view on some differences.

This is a good point. We have updated the discussion to provide some guidance. One likely reason for differences—when they exist—is that soot of varying maturity was accessed in a given study. As is suggested by Fig. 3 and the discussion in Section 5.1.3 (and in the response to the next comment), the MAC likely increases with maturation. Thus, in cases where literature MAC values are on the lower side, it could reflect sampling of less mature soot. Of course, differences could simply result from experimental uncertainty and historical challenges in measuring both BC concentrations and absorption accurately.

While these data support the conclusion presented in the abstract, it appears from Figure 3 that RDG theory over-predicts the MAC at smaller particle sizes when Mie Theory appears to do a better job, would a combination of these two separate approaches result in a better parameterization? It seems to be that the problem with black carbon absorption may simply be shifted from an underestimation with Mie Theory to and overestimation with RDG.

While this is certainly possible, we believe that the more likely reason for the overestimate at small sizes results from challenges with generating particles with constant composition ("maturity") at all sizes using the flame generators here. This is directly related to the discussion of soot "maturity" in section 5.1.3. While we do not have definitive proof, we believe that had we been able to sample soot of a constant maturity at all sizes we would have observed a constant (size-independent) MAC. Soot maturity has been studied for flames and fuels such as that used here by others (Johansson et al., 2017;Leschowski et al., 2015;López-Yglesias et al., 2014). The work by Johansson et al. (2017) suggests that the absorption cross-section (and thus the MAC) increases with maturity, consistent with our observations. Additionally, they note that the wavelength dependence of absorption is steeper (higher AAE) for less mature soot. This is consistent with our observations in Fig. 4, where there is, perhaps, a slight downward trend in the AAE with particle size.

An important question is, of course, what is the maturity of soot produced from diesel engines and biomass combustion, does it vary with size, and how does it relate to the soot produced here? As we noted, “flame-generated BC particles have been shown to be a suitable proxy for atmospheric BC particles, both in terms of chemical bonding and structural properties (Slowik et al., 2007;Hopkins et al., 2007).” However, the question of size-dependent maturity for diesel and biomass burning particles is unresolved. Yon et al. (2011)investigated soot produced from combustion of diesel fuel, albeit produced from a flame generator and not an engine, but did not look at the size dependence. Their results do, however, suggest that the soot from diesel soot can be considered reasonably mature.

It’s noted in the conclusions that future works will consider coatings, I look forward to seeing this work.

Indeed. We hope to have this completed soon.

Specific comments

Pg 2, Line 6: consider defining Mie size parameter explicitly.

We have added an explicit definition here, and on page 12. “(*The dimensionless size parameter* $x = \pi d_p/\lambda$*, where* d_p *is particle diameter and l is wavelength*.)”

Pg 3, Line 19: ‘fuller’ seems out of place, perhaps ‘more complete’?

We have updated to “*more thorough*.”

Pg 4, Line 10: what is the associated uncertainty the fuel equivalence ratio?

We have updated this as follows:

> “During BC3, BC3+, and BC4, most experiments were conducted using particles produced from an inverted co-flow diffusion flame operating on methane with a sheath flow mixture of O_2 and N_2 (Stipe et al., 2005) with a net fuel equivalence ratio, ϕ, = 0.7 *± 0.07; because the diffusion flame entrains sheath oxygen into the methane-rich center flow a range of* ϕ *values are accessed including regions where the local* ϕ *may be greater than 1*.”

Pg 8, Line 4: ‘size-selected’, mobility selected?

Yes. We have clarified to now state “*DMA* size-selected.”

Pg 8, Line 4: Which soot, i.e. what lot from which company? There is a certain amount of variability?

We now report that we used Alfa Aesar Lot L18U002.

Pg 8, Line 4: Was any coating analysis performed on the data collected from the SP2?

No, we did not perform coating analysis using the SP2 for this study. The laboratory environment allowed us to constrain the amount of coating using the CPMA.

Pg 9, Line 18: perhaps citing the original paper (Park et al. 2004 I believe, there may have been one earlier that used the formulation shown in this manuscript) that brought up the Df,m mobility shape factor would be more appropriate than Cross et al. 2010.

We now cite Park et al. (2003), who report this relationship.

Pg 12, Section 5.1.1: As I understand, the methane diffusion flame was used in BC3, BC3+, and BC4. Can you explain why the Df described here is different than that of the Df described in Bhandari et al., 2016? I would expect nascent soot particles to have a lower mass mobility exponent.

First, we have updated this reference to Bhandari et al. (2017). There is fundamental difference between the fractal dimension (what Bhandari et al measure) and the mass-mobility exponent (what is measured in this study). The difference between the two is described in detail by Sorensen (2011). The fractal dimension of typical soot is on the order of ~1.8; the mass-mobility exponent of typical uncoated soot is on the order of ~2.5 (e.g. Figure 3 in Olfert et al. (2017)). Thus we fully expect the fractal dimension measured by Bhandari (2017) to be lower than the mass-mobility exponent measured here.

To the reviewer's question, the difference likely results from different methods of determination. Bhandari et al. (2017) determined the Df (fractal dimension) values from analysis of SEM images and by fitting a line to the number of spherules comprising a particle versus dimensions of the particle (specifically $\sqrt{(L \cdot W)/d_p}$ where L and W are the length and width of the overall particle and d_p is the spherule diameter). In contrast, we determined Df,m (mass mobility exponent) from plots of per-particle mass versus mobility diameter.

We have added the following to Section 4.1: "(The mass mobility exponent, $D_{f,m}$, differs from the fractal dimension, D_f, as discussed by Sorensen (2011).)"

Pg 13, Line 27: It appears that Mie also overestimates at smaller particle sizes as well.

We have updated this sentence to clarify: "When the fits are restricted to $x < 0.9$, a reasonable fit using Mie theory is obtained at all wavelengths over this size range, *although there is perhaps a small overestimate at the smallest sizes*."

Pg 14, Line 6: Can you comment on why these RI values are larger than those used in current global climate models?

In short, because many models have adopted the values of Bond and Bergstrom (2006), and their suggested RI yields MAC values at many sizes lower than is supported by observations. We have added the following for clarification: "For reference, using *RI* = 1.95 – 0.79*i* the *MAC* at 532 nm calculated for BC in the small particle limit (assuming a material density of 1.8 g/cm^3) is only 5.1 m^2 g^{-1}, but peaks at 7.5 m^2 g^{-1} around $d_{\text{p,VED}}$ = 150 nm."

For additional consideration, the value suggested by Bond and Bergstrom (2006) was arrived at after consideration of a variety of literature measurements of soots of various types, and with measurements made in many different ways. They determined a value of 1.95 – 0.79*i* by matching, approximately, a model that accounts for varying "void fractions" with a suite of the observations, and finding where this intersects with an estimate of how the refractive index varies with extent of "graphitization." They ultimately state that "The value 1.95–0.79i merely provides agreement with many of the measurements."

Pg 14, Line 8: Specify that this recommendation is for 550 nm.

It is our understanding that the RI reported by Bond and Bergstrom (2006) is not for a specific wavelength, but is meant to be general. The references used to derive the RI do not all use 550 nm. The recommended MAC value is, however, wavelength-specific.

Pg 14-15, Line various: considerable time is spent discussing the MAC values in context with other literature, but there is little comment as to why these differences may exist.

We think the most likely reason for differences is differences in soot maturity. We have added a sentence to this effect. "One key reason that differences may exist between studies is that the BC particles sampled had differing maturity. Soot maturity refers to the extent to which the BC has a more disordered internal structure with high hydrogen content (low maturity) versus a more ordered, graphite-like structure with low hydrogen content (high maturity) (Johansson et al., 2017). The absorption cross-section for BC likely increases with increasing soot maturity (López-Yglesias et al., 2014)."

Pg 17, Line 16: I suggest adding this note "RI fitting was performed. . ." to the caption in Figure 3.

We have updated Fig. 3 caption.

Pg 19, Line 1: Could information regarding the soot maturity be accessed using LEO- fitting analysis with the SP2? At least that would indicate coating thickness which would indicate atmospheric processing.

To clarify, the concept of "soot maturity" is not related to how coated (or not) a particle is, but to the properties of the BC material (see above). As such, LEO-fitting would not be especially helpful.

Figure 2: As presented the fits are hidden behind the data, please bring them to the front to allow the reader to clearly see them. Perhaps a bottom panel showing the % difference or some such metric

indicating the deviation from model vs measurement below each plot to clearly identify differences between Mie and RDG could be helpful?

We have updated Fig. 2 to move the fit lines to the front. We have not added additional % difference plots because Fig. 3 shows the transformation of the data in Fig. 2 to MAC space, and we think that this further helps to illustrate the differences.

Response to Reviewer #2

The manuscript presents a thorough description of optical property measurements con- ducted during a series of experiments examining soot emissions from two different types of flames. It presents a detailed analysis of the merits of Mie and RDG ap- proximations of uncoated soot optical properties, and explores implications for climate models. The experiments and measurements are of a high quality and provide an ex- tremely useful collection of data for interpretation of similar measurements performed for other BC emission sources. They raise important questions regarding treatment of BC in climate models, and I look forward to their future work related to coated BC properties

I recommend its publication in ACP with only a few minor corrections, listed below.

The reference in the introduction giving an upper end estimate of potential BC forcing is now 10 years old, and this section would benefit form including one or two more recent estimates, though I understand the authors are pointing out an extreme case.

We have updated this as follows:

> "The exact magnitude of the climate impacts of BC remain uncertain. One estimate puts top-of-the-atmosphere direct forcing by BC as high as 0.9 W m^{-2}, which is comparable in magnitude to that of CO_2 (Ramanathan and Carmichael, 2008). Other more recent assessments yield 0.71 W m^{-2} with 90% uncertainty bounds of 0.08 to 1.27 W m^{-2} (Bond et al., 2013) or 0.61 [+0.16 to +1.40] W m^{-2} (Wang et al., 2016), while the IPCC suggests a value of 0.40 [+0.05 to +0.80] W m^{-2} (Boucher et al., 2013)."

Page 8, line 4: please be specific as to what "size" is referring to here...mobility diam- eter or mass.

We now state "DMA size selected" to clarify.

Page 8, line 22: stating truncation angles for the CAPS-SSA here would be helpful.

Rather than giving the truncation angles, we now state the magnitude of the correction based on (Onasch et al., 2015b).

> "The CAPS PM_{SSA} measures b_{sca} using an integrating nephelometer, corrected for the finite viewing angle of the detector, i.e. truncation correction (Onasch et al., 2015b). *The truncation*

> *correction at 630 nm was determined to be <1% at 630 nm for particles smaller than 300 nm, increasing to <5% for particles smaller than 800 nm*."

Page 9 - i believe the equations for MAC should have units of area, not inverse Mm

We think the reviewer meant cross-sections, not MAC. We have updated the manuscript.

Response to Reviewer #3

This is a well written article and present the solid absorption result using the well con- strained soot source and the result is straightforward for models to pick up. but it would even more benefit the community if addressing the following points:

-how could flame soot represent the ambient soot, in terms of refractive index and particle morphology? Then how could be suggested these results could be widely used in the model?

-if we have a different source of BC, for example the biomass burning, how could we guarantee the RI still the same?

We address the above two points together. While we do not have direct evidence that the BC produced from our flames is guaranteed to have the same RI as ambient soot, we point to the references of Hopkins et al. (2007) and Slowik et al. (2007) as support for the lab soot and ambient soot having similar properties. As we previously stated:

> "Although atmospheric BC particles are predominately generated through combustion of fossil fuels or through biomass burning (Bond et al., 2013), flame-generated BC particles have been shown to be a suitable proxy for atmospheric BC particles, both in terms of chemical bonding and structural properties (Slowik et al., 2007;Hopkins et al., 2007)."

We have expanded this discussion (in Section 5.1.3) to include additional details:

> "For example, Hopkins et al. (2007) find that the sp^2 content of ethylene and methane flame soot are similar to diesel soot (63%, 60%, and 56%, respectively), and have similar aromatic content. There is also a reasonable similarity between SP-AMS mass spectra of flame soot and soot particles in diesel exhaust or smoke from biomass burning (Onasch et al., 2015a)."

-It would be better to show the mass distribution of DMA-selected particles at different cases (to indicate the width of the distribution), as the single particle mass is crucial for the following analysis.

We now report typical geometric standard deviations ($\sigma_{g,CPMA}$) in the measured per-particle mass from the CPMA. For "forward-coating" experiments, the typical $\sigma_{g,CPMA}$ was 1.3. For "reverse-coating" experiments, the $\sigma_{g,CPMA}$ were generally larger, ranging from around 1.3 to 2. Based on the reviewers concern, we have examined whether there is any dependence of the measured MAC values on the

$\sigma_{g,CPMA}$. Using data from BC4 as an example, we find no significant dependence of the measured MAC values on $\sigma_{g,CPMA}$, with a linear fit between MAC and $\sigma_{g,CPMA}$ giving an $r^2 < 0.01$ and a slope at 532 nm (for example) of -0.08 +/- 0.7. We now state in Section 3.2 that:

"The typical geometric standard deviation of the per-particle mass distributions for forward-coating experiments was 1.3, while for reverse-coating experiments it ranged from around 1.3 to 2."

And in section 5.1.1 we now state that:

"For the reverse-coating experiments, which gave broader BC per-particle mass distributions compared to forward-coating distributions, we found no dependence of the derived MAC values on the distribution width."

-how have you proven the TD 5secs soot is nascent or no re-condensation down the pipe? Maybe showing some mass spectra to prove these are all refractory BC will be useful. And this also concerns the coated and then denuded soot.

The removal of coating material was demonstrated for BC2 by Cross et al. (2010) for these coating materials, and is further supported by the literature. While we could add a few spectra if deemed really necessary, we think that it is sufficient to add the following statement in Section 3.2: *"Literature results indicate that thermodenuding of particles coated with or composed of these materials leads to essentially complete evaporation of the non-refractory material (Cappa and Wilson, 2011;Huffman et al., 2008), confirmed by measurements from BC2 (Cross et al., 2010)."*

-It was mentioned you have used three PASS instruments, how were they compared with each other? better to show in a plot maybe.

This was only the case for the BC2 study, and is already discussed in Cross et al. (2010). Rather than repeat this analysis, we now point the reader to this reference.

-Fig. S4, could we change the colour scale a bit show the minima of X2.

For the RDG fits, the solution surface is very flat and there are many values that yield equivalently good fits to the observations. We show below Fig. S4A with the original scale (left) and an extremely narrowed scale (right). Even with changing the scale, the minima in the surface is not evident. The key point is that there is not a single solution for the RDG fits. As we stated in the main text:

"In contrast, fits performed using the RDG approximation do not give a unique set of *m* and *k*, but instead a band of [*m*,*k*] pairs that describe the data equally well (Figure S4). Since RDG fits are non-unique, optimal *k* values are reported at all wavelengths for a fixed value of *m* = 1.80."

As such, we have not updated the figures. We have, however, updated the caption to indicate that the crosses for the RDG fits were selected where *m* = 1.80.

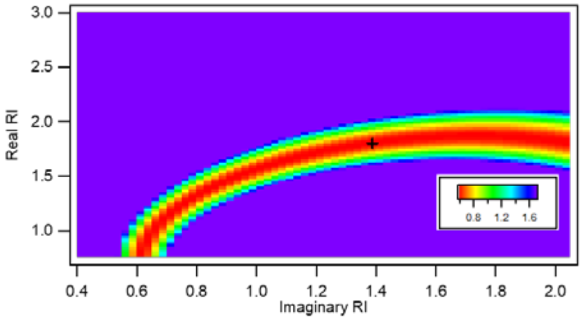

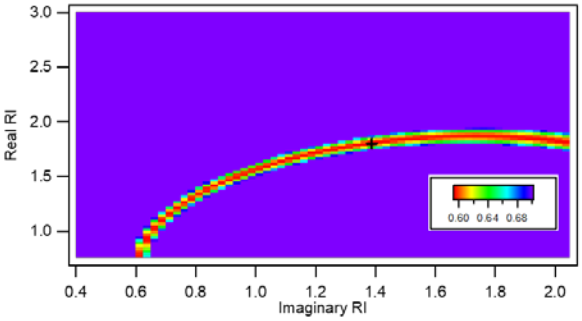

-there is no label for Fig. S8.

Perhaps there was a pdf rendering problem? We downloaded the supplement and can see the figure caption for Fig. S8.

-one important information is how the size parameter could relate to the volume equivalent diameter. For a general practice, could we assume >160nm BC will have a MAC using RDG approach, and how this VED will depend on the wavelength.

The size parameter relates to the volume equivalent diameter as: $x = \pi d_{p,VED}/\lambda$. We now give this definition explicitly. Yes, for larger particles it can be assumed that the MAC of BC can be represented using an RDG approach. This is equivalent to assuming a constant MAC, as we conclude in the last sentence of our abstract.

References

Bhandari, J., China, S., Onasch, T., Wolff, L., Lambe, A., Davidovits, P., Cross, E., Ahern, A., Olfert, J., Dubey, M., and Mazzoleni, C.: Effect of Thermodenuding on the Structure of Nascent Flame Soot Aggregates, Atmosphere, 8, 166, 10.3390/atmos8090166, 2017.

Bond, T. C., and Bergstrom, R. W.: Light Absorption by Carbonaceous Particles: An Investigative Review, Aerosol Science and Technology, 40, 27-67, 10.1080/02786820500421521, 2006.

Bond, T. C., Doherty, S. J., Fahey, D. W., Forster, P. M., Berntsen, T., DeAngelo, B. J., Flanner, M. G., Ghan, S., Kärcher, B., Koch, D., Kinne, S., Kondo, Y., Quinn, P. K., Sarofim, M. C., Schultz, M. G., Schulz, M., Venkataraman, C., Zhang, H., Zhang, S., Bellouin, N., Guttikunda, S. K., Hopke, P. K., Jacobson, M. Z., Kaiser, J. W., Klimont, Z., Lohmann, U., Schwarz, J. P., Shindell, D., Storelvmo, T., Warren, S. G., and Zender, C. S.: Bounding the role of black carbon in the climate system: A scientific assessment, Journal of Geophysical Research: Atmospheres, 118, 5380-5552, 10.1002/jgrd.50171, 2013.

Boucher, O., Randall, D., Artaxo, P., Bretherton, C., Feingold, G., Forster, P., Kerminen, V.-M., Kondo, Y., Liao, H., Lohmann, U., Rasch, P., Satheesh, S. K., Sherwood, S., Stevens, B., and Zhang, X. Y.: Clouds and Aerosols, in: Climate Change 2013: The Physical Science Basis. Contribution of Working Group I to the Fifth Assessment Report of the Intergovernmental Panel on Climate Change, edited by: Stocker, T. F., Qin, D., Plattner, G.-K., Tignor, M., Allen, S. K., Boschung, J., Nauels, A., Xia, Y., Bex, V., and Midgley, P. M., Cambridge University Press, Cambridge, United Kingdom and New York, NY, USA, 571-658, 2013.

Cappa, C. D., and Wilson, K. R.: Evolution of organic aerosol mass spectra upon heating: implications for OA phase and partitioning behavior, Atmos. Chem. Phys., 11, 1895-2011, 10.5194/acp-11-1895-2011, 2011.

Cross, E. S., Onasch, T. B., Ahern, A., Wrobel, W., Slowik, J. G., Olfert, J., Lack, D. A., Massoli, P., Cappa, C. D., Schwarz, J. P., Spackman, J. R., Fahey, D. W., Sedlacek, A., Trimborn, A., Jayne, J. T., Freedman, A., Williams, L. R., Ng, N. L., Mazzoleni, C., Dubey, M., Brem, B., Kok, G., Subramanian, R., Freitag, S., Clarke, A., Thornhill, D., Marr, L. C., Kolb, C. E., Worsnop, D. R., and Davidovits, P.: Soot Particle Studies—Instrument Inter-Comparison—Project Overview, Aerosol Science and Technology, 44, 592-611, 10.1080/02786826.2010.482113, 2010.

Hopkins, R. J., Tivanski, A. V., Marten, B. D., and Gilles, M. K.: Chemical bonding and structure of black carbon reference materials and individual carbonaceous atmospheric aerosols, Journal of Aerosol Science, 38, 573-591, 10.1016/j.jaerosci.2007.03.009, 2007.

Huffman, J. A., Ziemann, P. J., Jayne, J. T., Worsnop, D. R., and Jimenez, J. L.: Development and characterization of a fast-stepping/scanning thermodenuder for chemically-resolved aerosol volatility measurements, Aerosol Sci. Technol., 42, 395-407, 10.1080/02786820802104981, 2008.

Johansson, K. O., El Gabaly, F., Schrader, P. E., Campbell, M. F., and Michelsen, H. A.: Evolution of maturity levels of the particle surface and bulk during soot growth and oxidation in a flame, Aerosol Science and Technology, 51, 1333-1344, 10.1080/02786826.2017.1355047, 2017.

Leschowski, M., Thomson, K. A., Snelling, D. R., Schulz, C., and Smallwood, G. J.: Combination of LII and extinction measurements for determination of soot volume fraction and estimation of soot maturity in non-premixed laminar flames, Applied Physics B, 119, 685-696, 10.1007/s00340-015-6092-2, 2015.

López-Yglesias, X., Schrader, P. E., and Michelsen, H. A.: Soot maturity and absorption cross sections, Journal of Aerosol Science, 75, 43-64, 10.1016/j.jaerosci.2014.04.011, 2014.

Olfert, J. S., Dickau, M., Momenimovahed, A., Saffaripour, M., Thomson, K., Smallwood, G., Stettler, M. E. J., Boies, A., Sevcenco, Y., Crayford, A., and Johnson, M.: Effective density and volatility of particles sampled from a helicopter gas turbine engine, Aerosol Science and Technology, 51, 704-714, 10.1080/02786826.2017.1292346, 2017.

Onasch, T. B., Fortner, E. C., Trimborn, A. M., Lambe, A. T., Tiwari, A. J., Marr, L. C., Corbin, J. C., Mensah, A. A., Williams, L. R., Davidovits, P., and Worsnop, D. R.: Investigations of SP-AMS Carbon Ion Distributions as a Function of Refractory Black Carbon Particle Type, Aerosol Science and Technology, 49, 409-422, 10.1080/02786826.2015.1039959, 2015a.

Onasch, T. B., Massoli, P., Kebabian, P. L., Hills, F. B., Bacon, F. W., and Freedman, A.: Single Scattering Albedo Monitor for Airborne Particulates, Aerosol Science and Technology, 49, 267-279, 10.1080/02786826.2015.1022248, 2015b.

Park, K., Cao, F., Kittelson, D. B., and McMurry, P. H.: Relationship between Particle Mass and Mobility for Diesel Exhaust Particles, Environmental Science & Technology, 37, 577-583, 10.1021/es025960v, 2003.

Ramanathan, V., and Carmichael, G.: Global and regional climate changes due to black carbon, Nature Geosci, 1, 221-227, 10.1038/ngeo156, 2008.

Slowik, J. G., Cross, E. S., Han, J.-H., Davidovits, P., Onasch, T. B., Jayne, J. T., WilliamS, L. R., Canagaratna, M. R., Worsnop, D. R., Chakrabarty, R. K., Moosmueller, H., Arnott, W. P., Schwarz, J. P., Gao, R.-S., Fahey, D. W., Kok, G. L., and Petzold, A.: An inter-comparison of instruments measuring black carbon content of soot particles, Aerosol Science and Technology, 41, 295-314, 10.1080/02786820701197078, 2007.

Sorensen, C. M.: The Mobility of Fractal Aggregates: A Review, Aerosol Science and Technology, 45, 765-779, 10.1080/02786826.2011.560909, 2011.

Stipe, C. B., Higgins, B. S., Lucas, D., Koshland, C. P., and Sawyer, R. F.: Inverted co-flow diffusion flame for producing soot, Review of Scientific Instruments, 76, 10.1063/1.1851492, 2005.

Wang, R., Balkanski, Y., Boucher, O., Ciais, P., Schuster, G. L., Chevallier, F., Samset, B. H., Liu, J., Piao, S., Valari, M., and Tao, S.: Estimation of global black carbon direct radiative forcing and its uncertainty constrained by observations, Journal of Geophysical Research: Atmospheres, 121, 5948-5971, doi:10.1002/2015JD024326, 2016.

Yon, J., Lemaire, R., Therssen, E., Desgroux, P., Coppalle, A., and Ren, K. F.: Examination of wavelength dependent soot optical properties of diesel and diesel/rapeseed methyl ester mixture by extinction spectra analysis and LII measurements, Applied Physics B, 104, 253-271, 10.1007/s00340-011-4416-4, 2011.

Measurement and modeling of the multi-wavelength optical properties of uncoated flame-generated soot

Sara D. Forestieri,[1, #] Taylor M. Helgestad[1,#] Andrew Lambe,[2,3] Lindsay Renbaum-Wolff[2], Daniel A. Lack,[4,5,^] Paola Massoli,[2] Eben S. Cross,[6,&] Manvendra K. Dubey,[7] Claudio Mazzoleni,[8] Jason Olfert,[9] Arthur Sedlacek,[10] Andrew Freedman,[2] Paul Davidovits,[3] Timothy B. Onasch,[2,3] Christopher D. Cappa[1]

[1]Department of Civil and Environmental Engineering, University of California, Davis, CA 95616
[2]Aerodyne Research Inc., Billerica, Massachusetts, USA, 01821
[3]Chemistry Department, Boston College, Boston, MA, USA, 02467
[4]NOAA Earth System Research Laboratory, Boulder, CO, USA, 80305
[5]University of Colorado, Cooperative Institute for Research of the Environmental Sciences, Boulder, CO, USA, 80305
[6]Department of Civil and Environmental Engineering, Massachusetts Institute of Technology, Cambridge, Massachusetts, USA
[7]Los Alamos National Laboratory, Los Alamos, NM, USA
[8]Deparment of Physics and Atmospheric Sciences Program, Michigan Technological University, Houghton, MI, USA
[9]Department of Mechanical Engineering, University of Alberta, Edmonton, Alberta, Canada
[10]Biological, Environmental and Climate Sciences Department, Brookhaven National Laboratory, Upton, New York, USA
[#] Now at: California Air Resources Board, Sacramento, CA, USA
[^] Now at: Transport Emissions, Air Quality and Climate Consulting, Brisbane, Australia
[&] Now at: Aerodyne Research Inc., Billerica, Massachusetts, USA, 01821

Correspondence to: Sara Forestieri (*sara.forestieri@arb.ca.gov*) or Christopher Cappa (cdcappa@ucdavis.edu)

1 Abstract

Optical properties of flame-generated black carbon (BC) containing soot particles were quantified at multiple wavelengths for particles produced using two different flames, a methane diffusion flame and an ethylene premixed flame. Measurements were made for: (i) nascent soot particles, (ii) thermally denuded nascent particles, and (iii) particles that were coated then thermally denuded, leading to collapse of the initially lacy, fractal-like morphology. The measured mass absorption coefficients (MAC) depended on soot maturity and generation, but were similar

Deleted:

Deleted:

between flames for similar conditions. For mature soot, here corresponding to particles with volume-equivalent diameters > ~160 nm, the MAC and absorption Angstrom exponent (AAE) values were independent of particle collapse while the single scatter albedo increased. The MAC values for these larger particles were also size-independent. The mean MAC value at 532 nm for larger particles was 9.1 ± 1.1 m^2 g^{-1}, about 17% higher than that recommended by Bond and Bergstrom (2006), and the AAE was close to unity. Effective, theory-specific complex refractive index (*RI*) values are derived from the observations with two widely-used methods: Lorenz-Mie theory and the Rayleigh-Debye-Gans (RDG) approximation. Mie theory systematically under-predicts the observed absorption cross-sections at all wavelengths for larger particles (with $x > 0.9$) independent of the complex *RI* used, while RDG provides good agreement. (The dimensionless size parameter $x = \pi d_p/\lambda$, where d_p is particle diameter and λ is wavelength.) Importantly, this implies that the use of Mie theory within air quality and climate models, as is common, likely leads to under-predictions in the absorption by BC, with the extent of under-prediction depending on the assumed BC size distribution and complex *RI* used. We suggest that it is more appropriate to assume a constant, size-independent (but wavelength-specific) *MAC* to represent absorption by uncoated BC particles within models.

Formatted: Font: Symbol

2 Introduction

Soot particles, which contain light-absorbing black carbon (BC), are a byproduct of incomplete combustion of fossil fuels and biomass. These particles affect climate directly by absorbing and scattering solar radiation (Bond et al., 2013) and indirectly by acting as cloud condensation nuclei, especially following chemical processing (Lohmann and Feichter, 2005). Soot particles absorb shortwave radiation and have an overall warming effect on climate. The exact magnitude of the climate impacts of BC remain uncertain. One estimate puts top-of-the-atmosphere direct forcing by BC as high as 0.9 W m^{-2}, which is comparable in magnitude to that of CO_2 (Ramanathan and Carmichael, 2008). Other more recent assessments yield 0.71 W m^{-2} with 90% uncertainty bounds of 0.08 to 1.27 W m^{-2} (Bond et al., 2013) or 0.61 [+0.16 to +1.40] W m^{-2} (Wang et al., 2016), while the IPCC suggests a value of 0.40 [+0.05 to +0.80] W m^{-2} (Boucher et al., 2013).

Deleted: Although t

Deleted: ,

Deleted: o

Deleted: (Boucher et al., 2013)

One challenge in modelling the optical properties of soot, and of the BC-component in particular, derives from BC having a complex, fractal-like structure, being an agglomerate of small "spherules" (Medalia and Heckman, 1969). One theory that is commonly used in climate models to calculate BC optical properties is Lorenz-Mie Theory (hereafter, Mie theory), which makes the physically unrealistic assumption that soot particles are spherical (Bohren, 1983). This theory is widely used in climate models (Bond et al., 2013) in part because it does not require any details about the number of spherules or the arrangement of the spherules within the agglomerate, but also because it is compatible with calculations for other spherical aerosol types. A variation on Mie theory, the Rayleigh-Debye-Gans (RDG) approximation, is also often used to model the optical properties of BC (Sorensen, 2001), albeit not by climate models. In RDG, the agglomerate absorption cross section (σ_{abs}) is the product of σ_{abs} for individual spherules and the number of spherules in the agglomerate. As such, RDG neglects spherule-to-spherule interactions and the mass absorption coefficient (*MAC*) of an individual spherule is equal to that of the overall particle. (The *MAC* is the absorption cross-section normalized by the particle mass.) There are more complex methods for calculating soot particle optical properties, including the T-matrix method (Mackowski and Mishchenko, 1996) and the discrete dipole approximation (DDA) (Purcell and Pennypacker, 1973), which account for interactions between spherules. Given that these more advanced methods require detailed information on the shape of the soot particles and are computationally intensive, they are not practical for climate models. The derived effective refractive indices used as inputs for these models are theory-specific and it is necessary to have experimentally constrained effective refractive indices for both RDG and Mie theory if they are to be employed in climate models. For example, Bond et al. (2006) suggested that BC can be described using an *MAC* = 7.5 m^2 g^{-1} at 550 nm and a complex *RI* = 1.95 – 0.79*i*. However, as they show, the maximum *MAC* calculated from Mie theory using this refractive index is only 7.2 m^2 g^{-1} over a very narrow range of particle sizes and is much smaller in general, with a value of 4.9 m^2 g^{-1} in the small particle limit, where RDG applies (assuming ρ = 1.8 g cm^{-3}). In other words, there can be an inconsistency between the oft used *MAC* and complex *RI*. This illustrates the need for theory-specific effective refractive index values and a more thorough exploration of the robustness of commonly used optical models.

Deleted: fuller

Our work investigates the ability of two optical models, Mie theory and the RDG approximation, to reproduce observed soot optical properties for particles composed primarily of BC. The observations include light absorption and extinction coefficients of soot particles produced from methane diffusion and ethylene premixed flames, measured over four different studies at multiple wavelengths. The impact of shape on soot particle optical properties is also examined. The soot particles sampled during these studies serve as a proxy for different types of soot particles in the ambient atmosphere. Recommended theory-specific complex RI values for BC-dominated soot particles are provided. However, we ultimately suggest that atmospheric models should consider adopting observationally constrained, wavelength-specific constant *MAC* values for BC rather than calculating the optical properties from optical theories.

3 Experimental: The Black Carbon Studies

The measurements reported here were made during a series of laboratory intensive studies that took place at Boston College (BC2, BC3 and BC4) in 2008, 2012 and 2015, respectively, and Aerodyne Research (BC3+) in 2014. Below, we provide details of soot particle generation and the measurements made. An experimental schematic is provided in Figure S1.

3.1 Soot particle generation

Soot particles were produced using two different flame sources and fuel types. During BC3, BC3+, and BC4, most experiments were conducted using particles produced from an inverted co-flow diffusion flame operating on methane with a sheath flow mixture of O_2 and N_2 (Stipe et al., 2005) with a net fuel equivalence ratio, ϕ, = 0.7 ± 0.07; because the diffusion flame entrains sheath oxygen into the methane-rich center flow a range of ϕ values are accessed including regions where the local ϕ may be greater than 1. These are referred to as the "methane diffusion flame" experiments, and have been combined into a single dataset since the sampling and generation were similar in all.

Deleted: .

During BC2 and for a small number of experiments during BC3+, particles were produced using a McKenna flat-flame burner from combusion of premixed C_2H_4 (ethylene), O_2 and N_2 with ϕ = 2.0 ± 0.2. These are referred to as the "ethylene premixed flame" experiments. Particles were sampled at a nominal height of 5 cm above the burner during BC3+, but at a nominal height of 20 cm above the burner during BC2 (Cross et al., 2010). As such, the results from the two ethylene premixed flame have been kept separate because particles were sampled from the flame differently in the two studies.

The soot particles produced from these two flames exhibited different properties. For example, the organic (OC) mass fraction of the nascent (i.e. freshly emitted and unprocessed) ethylene premixed flame soot particles in BC2 was ~0.26 (Cross et al., 2010), whereas the OC fraction of nascent methane diffusion flame particles was < 0.01. Consequently, upon heating to >200°C the per-particle mass of the ethylene premixed flame soot particles decreased while the methane diffusion flame soot particles were unaffected.

The sampling and/or burner conditions were modified during these studies to generate monodisperse soot particles volume equivalent diameter ($d_{\mathrm{p,VED}}$) less than 160 nm. The $d_{\mathrm{p,VED}}$ is the diameter calculated from the per-particle mass assuming that particles have spherical morphology and the material density of the particles is 1.8 g/cm^3 (Bond and Bergstrom, 2006;Wu et al., 1997;Mullins and Williams, 1987):

$$d_{p,VED} = \left(\frac{6m_p}{1.8\cdot\pi}\right)^{1/3} \qquad (1)$$

where m_{p} is the per-particle mass. For the ethylene premixed flame, sampling closer to the burner surface selected for smaller soot particles; sampling on the center line over the burner surface versus off-center may also affect the selected soot particle sizes. For the methane diffusion flame, increasing the fuel dilution (N_2) fraction generated smaller soot particles (Stipe et al., 2005). These variations in sampling and/or burner conditions likely led to some changes in the particle optical and chemical properties (López-Yglesias et al., 2014). Thus, some of the size-dependent changes observed in particles smaller than $d_{\mathrm{p,VED}}$ ~ 160 nm, discussed below, are likely a result of real changes in the particle properties. The extreme case is in the comparison between the soot particles sampled at 5.1 cm (BC3+) and 20.3 cm (BC2) above the ethylene premixed flame burner surface.

3.2 Particle Processing

The soot particles were subjected to various physical and chemical processing and were selected according to their mobility diameter after processing but prior to sampling for optical and chemical property measurements. Particles size selected with no processing are termed nascent soot particles. For some experiments, nascent particles were passed through a thermal denuder in which they were heated to 270°C for ~5 seconds. Such particles are termed nascent-denuded soot particles. (A summary of terminology is provided in Table S1.) For other experiments, nascent particles were first coated and then thermodenuded. Coating materials included either dioctyl sebacate (DOS, $C_xH_yO_x$; BC2, BC3, and BC3+), sulfuric acid (H_2SO_4; all studies), or secondary organic aerosol from α-pinene photooxidation (SOA; BC4). These particles are referred to as coated-denuded. Literature results indicate that thermodenuding of particles coated with or composed of these materials leads to essentially complete evaporation of the non-refractory material (Cappa and Wilson, 2011;Huffman et al., 2008), confirmed by measurements from BC2 (Cross et al., 2010).

Formatted: Subscript

For DOS coatings, the nascent particles were first size selected, the monodisperse nascent particles were coated, and the coated particles were subsequently denuded. This is referred to as a forward-coating experiment. For either H_2SO_4 or SOA coatings, polydisperse nascent soot particles were first coated, then size selected, and finally denuded. This is referred to as a reverse-coating experiment. This difference in methodology decreased the extent of homogenous nucleation of pure H_2SO_4 and SOA particles by providing additional soot surface area to act as a condensation sink, and any nucleated particles were further excluded during the size selection. However, the reverse method led to broader size and mass distributions in the denuded soot cores. The typical geometric standard deviation of the per-particle mass distributions for forward-coating experiments was 1.3, while for reverse-coating experiments it ranged from around 1.3 to 2.

For BC2, BC3, and BC3+, soot particles were coated in a heated section of tubing containing either DOS or H_2SO_4, which cooled and condensed onto soot particles after exiting the heated section of tubing. For BC4 experiments, soot particles were coated with α-pinene SOA and H_2SO_4 that were generated in a Potential Aerosol Mass (PAM) oxidation flow reactor (Lambe et al., 2011). In the PAM reactor, O_3 was photolyzed by UV lamps at $\lambda = 254$ nm to produce $O(^1D)$ radicals, which then reacted with water (RH=25-30%) to produce OH radicals. Low volatility products were formed via the reaction between OH and α-pinene, which condensed onto the soot particles. Similarly, H_2SO_4 was formed through the reaction of SO_2 and OH radicals.

Particles were size selected according to their mobility diameter (d_m) using a differential mobility analyser (DMA; TSI model 3080) with sheath-to-sample flow ratio of 5:1, yielding resolution of ~ ±20% of the set point in terms of mobility. During BC4, particles were mass-selected with a centrifugal particle mass analyser (CPMA; Cambustion Ltd.), in addition to being size-selected using a DMA. Particles sampled into the DMA or CPMA first passed through a neutralizer, which imparts an equilibrium charge distribution to the particles. The DMA selects particles according to their electrical mobility, which is dependent upon the number of charges per particle. Particles with more than one charge are larger than those with a single charge, and the presence of these larger particles can confound interpretation of optical property measurements. Altering the burner and sampling conditions for both flame types minimized the number of these multiply-charged particles during the experiments, and in some cases their concentrations were effectively zero. However, for some experiments, their concentrations were non-zero. The method used to account for the multiply-charged particles is discussed below.

3.3 Instrumentation

A wide range of instruments was employed to characterize the soot particle size, mass, composition and optical properties. Not all instruments were deployed for all studies, summarized in Table S2.

3.3.1 Size and Mass

Particle mobility size distributions were measured using a scanning mobility particle sizer (SMPS; TSI model 3936). Particles sampled into the SMPS were passed through a neutralizer, which imparts a new equilibrium charge distribution to the particles. This (re)neutralization step shifts the charge distribution of the monodisperse particles imparted by the size-selection DMA to a new equilibrium state. For particles with mobility diameters 200-300 nm (typical of these studies), the number concentration ratio between particles with +1 charge to those with a greater number of charges selected by the DMA is ~2-2.5 at equilibrium. Thus, after (re)neutralization, the majority of the particles that were in a +2 state coming out of the DMA are sized in the SMPS in their +1 state. This allows for quantitative determination of the fraction of particles that had charge states of +1, +2, +3, etc., when selected by the DMA. The information is used to correct the optical measurements for contributions from larger, multiply-charged particles for BC2, BC3, and BC3+.

Particle mass distributions were measured using a CPMA. Particle number concentrations were measured using a condensation particle counter (CPC; TSI Inc.) and using a mixing CPC (MCPC, BMI model l710). The two particle-counting instruments were placed at different points in the flow path to estimate and account for losses in the transfer lines between instruments. All CPCs number concentrations agreed within ± 5%.

3.3.2 Composition

Particle composition was characterized online using a soot particle aerosol mass spectrometer (SP-AMS; Aerodyne Research, Inc.) (Onasch et al., 2012) and a compact time-of-flight aerosol mass spectrometer (c-ToF-AMS; Aerodyne Research, Inc.) (Canagaratna et al., 2007). The SP-AMS measured concentrations of refractory BC and the associated refractory and non-refractory coatings in BC-containing particles. The c-ToF-AMS measures concentrations of only non-refractory materials, which include particulate organic matter (POM) and some inorganic salts (NH_4^+, SO_4^{2-}, NO_3^-). Both instruments allow for determination of mass-weighted particle size distributions as characterized by the vacuum aerodynamic diameter ($d_{\mathrm{p,va}}$). Particles were also collected on quartz-fiber filters for offline thermal-optical analysis (Chow et al., 2004), from which the relative abundances of OC and elemental carbon (EC) are determined.

During BC4, refractory black carbon mass was quantified with a single particle soot photometer (SP2; Droplet Measurement Technologies). The SP2 heats up the soot particles with an Nd:YAG laser and quantifies the incandescence emission as the particle evaporates. The incandescence signal from the instrument was calibrated using DMA size-selected fullerene soot (Alfa Aesar Lot L18U002) (Laborde et al., 2012). The mass distributions from the SP2 were used to determine contributions from multiply-charged particles during BC4.

3.3.3 Optical properties

Particle optical properties were characterized using multiple instruments. Three different photoacoustic spectrometers (PAS) were used during the various studies to measure particulate light absorption coefficients (b_{abs}). During BC2, a custom-built PAS from the National Oceanic and Atmospheric Administration (NOAA) operating at $\lambda = 532$ nm was deployed (Lack et al., 2006). Also, during BC2, a commercial 3-wavelength particle absorption soot spectrometer

(PASS-3; DMT, Inc.) operating at λ = 405 nm, 532 nm and 781 nm was deployed by Los Alamos National Laboratory (LANL) (Flowers et al., 2010). The results from the different PAS instruments for BC2 are compared in (Cross et al., 2010). During BC3, BC3+, and BC4, a custom-built PAS from the University of California, Davis (UCD) operating at λ =405 nm and 532 nm was deployed (Lack et al., 2011;Cappa et al., 2012). Light absorption was also measured during BC3, BC3+, and BC4 at λ = 630 nm using a commercial cavity attenuated phase-shift single scatter albedo spectrometer (CAPS PM_{SSA}; Aerodyne Research, Inc.). The CAPS PM_{SSA} measures particulate light absorption as the difference between the measured light extinction (b_{ext}) and scattering (b_{sca}) coefficients, whereas the PAS instruments measure light absorption directly. The CAPS extinction measurement has been previously described (Massoli et al., 2010). The CAPS PM_{SSA} measures b_{sca} using an integrating nephelometer, corrected for the finite viewing angle of the detector, i.e. truncation correction (Onasch et al., 2015b). The truncation correction at 630 nm was determined to be <1% at 630 nm for particles smaller than 300 nm, increasing to <5% for particles smaller than 800 nm. Light extinction coefficients were measured at λ = 532 nm during BC2 using the NOAA cavity ringdown (CRD) spectrometer, and at λ = 405 nm and 532 nm during BC3, BC3+, and BC4 using the UCD CRD spectrometer (Langridge et al., 2011). Light extinction coefficients were also determined during BC2 at λ =405 nm, 532 nm and 781 nm using the PASS-3 instrument, which, like the CAPS PM_{SSA}, incorporates an integrating nephelometer to measure b_{sca}; b_{ext} is determined as the sum of b_{abs} and b_{sca}.

Absorption and extinction cross sections were determined for the size-selected particles as:

$$\sigma_{abs}(m^2/particle) = \frac{b_{abs}}{N_p} \tag{2}$$

$$\sigma_{ext}(m^2/particle) = \frac{b_{ext}}{N_p} \tag{3}$$

Deleted: Mm^{-1}

where N_p is the measured particle number concentration. Additional parameters of interest that can be calculated from the measurements are the wavelength-dependent mass absorption and extinction coefficients, *MAC* and *MEC*, respectively, defined as:

$$MAC(m^2\ g^{-1}) = \frac{b_{abs}}{N_p \times m_p} \tag{4}$$

$$MEC(m^2\,g^{-1}) = \frac{b_{\mathrm{ext}}}{N_{\mathrm{p}} \times m_{\mathrm{p}}} \qquad (5)$$

where m_p is the per particle mass. The combination of the absorption and extinction cross-sections allows for calculation of single scatter albedo, defined as:

$$SSA = 1 - \frac{\sigma_{abs}}{\sigma_{ext}}. \qquad (6)$$

The *SSA* characterizes the fraction of extinction that is due to scattering. The wavelength-dependence of absorption is characterized by the semi-empirical parameter the absorption Ångström exponent, defined as:

$$AAE = \frac{\ln\left(\sigma_{abs,2}/\sigma_{abs,1}\right)}{\ln\left(\lambda_1/\lambda_2\right)} \qquad (7)$$

where λ is wavelength and the subscript 1 and 2 indicate two different wavelengths.

4 Data Analysis

4.1 Mass Mobility Exponent

One measure of particle shape is the mass mobility exponent ($D_{f,m}$) (Park et al., 2003):

Deleted: (Cross et al., 2010)

$$m_p = C \cdot d_m{}^{D_{f\_m}} \qquad (8)$$

where *C* is the proportionality constant. (The mass mobility exponent, $D_{f,m}$, differs from the fractal dimension, D_f, as discussed by Sorensen (2011).) Values of $D_{f,m}$ for atmospheric particles typically range from 2.0 to 3.0, with lower values being characteristic of more "lacy" soot and higher values of more compacted soot. $D_{f,m}$ values were obtained for nascent and coated-denuded soot particles by fitting a power law function to a graph of m_p versus d_m.

4.2 Refractive Index Retrieval

Effective complex refractive index values (RI; $n = m + ki$) for the soot particles were determined using two methods: (1) spherical particle Mie Theory and (2) Rayleigh-Debye-Gans (RDG) approximation. For the refractive index, *m* is the real component and *k* is the imaginary component.

In Mie Theory, particle cross-sections are calculated assuming spherical particles with a homogeneously uniform complex refractive index. The calculated cross-section is the product of the calculated absorption or extinction efficiency (Q_{abs} or Q_{ext}) and the geometric particle cross-section ($= \pi \cdot [d_{\mathrm{p}}/2]^2$, where d_{p} is the particle diameter). Here, the particle diameter used in the calculations is the measured $d_{p,\mathrm{VED}}$, as determined from the CPMA per-particle mass measurements and assuming a material density for BC of 1.8 g/cm^3. In the RDG approximation (Sorensen, 2001), the absorption cross-sections are calculated as:

$$\sigma_{abs,RDG} = N_{spherule}\sigma_{\mathrm{abs,spherule}} \tag{9}$$

where N_{spherule} is the number of spherules comprising a particle and $\sigma_{\mathrm{abs,spherule}}$ is the absorption cross-section calculated for a single spherule using Mie theory. Here, we have assumed that $N_{\mathrm{spherule}} = m_{\mathrm{p}}/m_{\mathrm{spherule}}$, where m_{p} is the measured per-particle mass and m_{spherule} is the mass of an individual spherule with $d_{\mathrm{p}} = 20$ nm (ethylene premixed flame) (Cross et al., 2010) or $d_{\mathrm{p}} = 37$ nm (methane diffusion flame) (Ghazi et al., 2013), again assuming a material density of 1.8 g/cm^3.

Optimal (best-fit), theory specific values of m and k were established by comparing the size-dependent observations of σ_{abs} to calculations from either Mie theory or the RDG approximation by varying these parameters over the ranges $1.3 < m < 2.2$ and $0.1 < k < 1.5$ and determining the minimum value of the reduced chi-square statistic:

$$\chi^2_{red} = \frac{1}{N-1}\sum_j \left[\frac{\left(\sigma^j_{abs} - \sigma^j_{abs,calc}\right)^2}{\varepsilon_{abs}{}^2} \right] \tag{10}$$

where $\sigma^{\mathrm{j}}_{\mathrm{abs}}$ is the measured absorption cross-section, $\sigma^{\mathrm{j}}_{\mathrm{abs,\ Mie}}$ is the calculated absorption cross-section, N is the number of points and $\varepsilon_{\mathrm{abs}}$ is the estimated uncertainty, which accounts for both instrumental uncertainties plus the uncertainty associated with contributions from multiply-charged particles. Individual fits were performed for each wavelength for each flame type. The methane diffusion flame soot data collected during different studies was treated as one dataset, whereas the ethylene premixed flame soot data collected during the different studies were kept separate due to the sampling differences described above.

4.3 Accounting for multiply charged particles

All absorption and extinction coefficient measurements were corrected for contributions from doubly-charged (Q2) particles. This correction leads to a decrease in the measured absorption and extinction coefficients. Here, an approach is taken where the fraction of absorption or extinction from Q2s ($f_{\mathrm{abs,Q2}}$ or $f_{\mathrm{ext,Q2}}$, respectively) is estimated from the measurements of the number fraction of singly and doubly charged particles (f_{Q1} and f_{Q2}, respectively) determined from either the SMPS (BC2, BC3, and BC3+) or the SP2 (BC4), the per-particle mass of singly and doubly charged particles ($m_{\mathrm{p,Q1}}$ and $m_{\mathrm{p,Q2}}$, respectively) and with an assumption of spherical particles (i.e. that $m_{\mathrm{p}} = \rho(\pi/6)d_{\mathrm{p,VED}}^3$), and that the *MAC* and *MEC* are size independent. The resulting expression for $f_{\mathrm{abs,Q2}}$ is then:

$$f_{abs,Q2} = \frac{f_{Q2}\cdot m_{p,Q2}\cdot MAC}{f_{Q1}\cdot m_{p,Q1}\cdot MAC + f_{Q2}\cdot m_{p,Q2}\cdot MAC} = \frac{f_{Q2}\cdot m_{p,Q2}}{f_{Q1}\cdot m_{p,Q1} + (1-f_{Q1})\cdot m_{p,Q2}} \sim \frac{f_{Q2}\cdot d^3_{p,VED,Q2}}{f_{Q1}\cdot d^3_{p,VED,Q1} + (1-f_{Q1})\cdot d^3_{p,VED,Q2}} \tag{11}$$

It is important to note that the final expression is independent of the absolute value of the *MAC*. A similar procedure was used to correct *MEC* values. Although the *MAC* (and *MEC*) may not be fundamentally size-independent, as assumed, the correction is relatively insensitive to differences in the *MAC* between sizes. For the size range of interest, there is a relatively constant relationship between the diameters of the singly- and doubly-charged particles, with $d_{\mathrm{p,VED,Q2}} \sim 1.6 d_{\mathrm{p,VED,Q1}}$ corresponding to $m_{\mathrm{p,Q2}} \sim 4 m_{\mathrm{p,Q1}}$. Thus,

$$f_{abs,Q2} \sim \frac{4(1-f_{Q1})}{f_{Q1}+4(1-f_{Q1})}\ , \tag{12}$$

and the absorption by Q1 particles only is:

$$b_{abs,Q1} = b_{abs,obs}(1 - f_{abs,Q2}). \tag{13}$$

As an example, if $f_{\mathrm{Q1}} = 0.95$ then $f_{\mathrm{abs,Q2}} = 0.17$, and the sensitivity of $f_{\mathrm{abs,Q2}}$ to uncertainties in f_{Q1} is $\delta f_{\mathrm{abs,Q2}} \sim 3\cdot\delta f_{\mathrm{Q1}}$, as determined by sensitivity calculations. We estimate the uncertainty in f_{Q1} is 0.01, which contributes ~3% to the uncertainty in $b_{\mathrm{abs,Q1}}$. (If the *MAC* were not constant, but were instead 20% larger for Q2s compared to Q1s, then the correction would increase to 0.20 from 0.17.) For most runs, the Q2 contribution was small, being 5% or less.

5 Results and Discussion

Results from the methane diffusion flame and from the two different ethylene premixed flame experiments are presented and discussed separately. For each flame type or configuration, the coated-denuded data for all coating types are considered together.

5.1 Soot optical properties from the methane diffusion flame

5.1.1 MAC values of nascent and coated-denuded soot

Average and median *MAC* values were determined for BC particles from the methane diffusion flame with $x > 0.9$ (corresponding to a $d_{p,\mathrm{VED}}$ = 160 nm at $\lambda = 532$ nm; Table S3). (The dimensionless size parameter $x = \pi d_p/\lambda$, where d_p is particle diameter and λ is wavelength.) There are no systematic differences in the *MAC* values between nascent and nascent-denuded ($D_{f,m} = 2.16 \pm 0.1$) and coated-denuded ($D_{f,m} = 2.64 \pm 0.1$) soot at any wavelength for this range of x despite some degree of collapse for the thickly coated-denuded particles (Figure 1 and Figure S2). The average *MAC* values for $x > 0.9$ were 12.1 ± 1.4 $\mathrm{m^2\,g^{-1}}$ at 405 nm, 9.1 ± 1.1 $\mathrm{m^2\,g^{-1}}$ at 532 nm and 7.1 ± 1.1 $\mathrm{m^2\,g^{-1}}$ at 630 nm, where uncertainties are 1σ standard deviations of the measurements. For the reverse-coating experiments, which gave broader BC per-particle mass distributions compared to forward-coating distributions, we found no dependence of the derived *MAC* values on the distribution width. The collapse was presumably due to the effect of evaporation or condensation of the coating material, and not due to the denuding process alone (Bhandari et al., 2017). The observed $D_{f,m}$-independence of the $MAC(x>0.9)$ is consistent with Radney et al. (2014). This contrasts, however, with modelling studies that use non-Mie based methods that can account for particle shape effects, which indicate "lacy" soot (with a fractal dimension, as opposed to mass mobility exponent, of $D_f = 1.8$) is more absorbing than "compact" soot ($D_f = 2.4$) (Kahnert and Devasthale, 2011;Scarnato et al., 2013). In the calculations, the compact soot particles are less absorbing because the inner-most spherules are "shielded" by the outer-most spherules. It is possible that the extent of collapse here was insufficient to lead to substantial "shielding" in our

Deleted: Figure 1

Formatted: Font: Not Bold

Formatted: Font: Symbol

Deleted: (Bhandari et al., 2016)

Deleted: ,m

Deleted: ,m

experiments. Regardless, given the similarity of the observed nascent and coated-denuded particle cross-sections, they have been recombined into a single dataset in what follows.

5.1.2 *RI values calculated from Mie Theory and the RDG approximation*

The σ_{abs} have been fit separately using Mie theory and the RDG approximation to determine optimal, theory-specific effective complex *RI* values. The observations and best fits are shown in Figure 2 at the three wavelengths (λ =405 nm, 532 nm, and 630 nm), and the derived optimal wavelength-, flame- and theory-specific values are reported in Table 1. The quality of the best fit obtained is dependent upon both theory and wavelength considered. First, fits performed using Mie theory tend to give reasonably well-defined minima in the calculated χ^2_{red}, indicating that the optimal *m* and *k* are unique (Figure S3). In contrast, fits performed using the RDG approximation do not give a unique set of *m* and *k*, but instead a band of [*m*,*k*] pairs that describe the data equally well (Figure S4). Since RDG fits are non-unique, optimal *k* values are reported at all wavelengths for a fixed value of *m* = 1.80.

Deleted: Figure 2

Formatted: Font: Not Bold

Deleted: Table 1

Formatted: Font: Not Bold

There are additional differences between Mie and RDG beyond the uniqueness of the derived optimal *RI*. At λ = 405 nm, Mie theory provides a poor fit to the σ_{abs} when the fit is performed using data over the entire size range sampled. In particular, at λ = 405 nm the σ_{abs} from Mie theory are overestimated below $d_{p,VED}$ ~120 nm (x ~ 0.9) and underestimated for larger sizes (Figure 2A). At λ = 532 nm, this deviation also occurs at x ~ 0.9 ($d_{p,VED}$ > 160 nm) corresponding to larger size particles. Compared to 405 nm, the overestimate at small *x* and underestimate at larger *x* for 532 nm is smaller. At λ = 630 nm, the Mie theory fit compares well with the observations at x < 0.9 ($d_{p,VED}$ ~ 180 nm) and with some deviation observed at larger sizes. When the fits are restricted to x < 0.9, a reasonable fit using Mie theory is obtained at all wavelengths over this size range, although there is perhaps a small overestimate at the smallest sizes. However, these constrained Mie fits extrapolated to larger sizes (x > 0.9) still underestimate the observed absorption. For RDG, generally good fits are obtained at all wavelengths and across all sizes, although the RDG-calculated σ_{abs} tend to overestimate the observation at smaller sizes below $d_{p,VED}$ ~100 nm.

Formatted: Font: Not Bold

Deleted: Figure 2

It is important to note that the *RI* values listed in Table 1 are theory and property specific. This means that the Mie-derived *RI* values are not appropriate for use with the RDG approximation,

Deleted: Table 1

Formatted: Font: Not Bold

and vice versa. Additionally, they must be used assuming a material density of 1.8 g/cm^3, since this value was used to convert m_p to $d_{\mathrm{p,VED}}$ or N_{spherule}. If, for example, a smaller density were used with these RI values then the particles would have substantially higher *MAC*s. Of note is that both the real and imaginary *RI*s from Mie theory are larger than *RI* values that are commonly used in global climate models (Bond et al., 2013), including the *RI* that is often considered the currently recommended value (1.95 – 0.79*i*) (Bond and Bergstrom, 2006). For reference, using *RI* = 1.95 – 0.79*i* the *MAC* at 532 nm calculated for BC in the small particle limit (assuming a material density of 1.8 g/cm^3) is only 5.1 m^2 g^{-1}, but peaks at 7.5 m^2 g^{-1} around $d_{\mathrm{p,VED}}$ = 150 nm.

5.1.3 Comparison of measured and calculated MAC values

Another way to look at the extent to which Mie theory or the RDG approximation can reproduce the observations is to compare the observed and calculated *MAC* values as a function of particle size (or *x*), rather than the σ_{abs} versus size relationship (as in Figure 2). Although the *MAC* is related directly to the σ_{abs}, it is nonetheless useful to consider the *MAC* values because they vary over a much narrower range than do the σ_{abs}. The dependence of the *MAC* on $d_{\mathrm{p,VED}}$ and size parameter for both the observations and the models are shown in Figure 3. The observed *MAC* values generally increase with $d_{\mathrm{p,VED}}$ or size parameter at all wavelengths up to around $d_{\mathrm{p,VED}}$ ~ 160 nm, above which they plateaus and are approximately constant. The ranges (minimum and maximum) of binned observed *MAC*s are provided in Table S4.

The *MAC* values observed here (Table S3) are substantially larger than the value of 5.7 ± 0.8 m^2 g^{-1} at λ = 405 nm reported by Radney et al. (2014), who use a Santoro-type burner (i.e., co-flow diffusion flame). They did not report any notable size dependence to their *MAC* values. Our *MAC* values (especially for $x > 0.5$) compare well with the value of 8.16 m^{2}g^{-1} at λ = 532 reported by You et al. (2016) (extrapolated from 7.89 ± 0.25 m^{2}g^{-1} at λ = 550 nm) for soot particles generated from the combustion of organic fuel stock over the $d_{\mathrm{p,VED}}$ range ~80 nm to ~210 nm. They also compare favorably to the range of values 7.2 to 8.5 m^{2}g^{-1} reported for λ = 532 nm for $d_{\mathrm{p,VED}}$ ~100 nm observed in Saliba et al. (2016) for particles generated from a cookstove. Some particle size dependence was reported by Khalizov et al. (2009), who used propane with a Santoro-type burner, with reported *MAC*s at λ = 532 nm of 6.7 ± 0.7 m^{2}g^{-1} for d_m = 155 nm particles and 8.7 ± 0.1 m^{2}g^{-1} for d_m = 320 nm particles. This general behavior was also observed for soot particles generated

Deleted: ,

Formatted: Font: Italic

Deleted: Figure 2

Formatted: Font: Not Bold

Formatted: Font: Not Bold

Deleted: Figure 3

from a methane diffusion flame in Dastanpour et al. (2017), with *MAC*s values reported at λ = 660 nm of ~5 $m^2\ g^{-1}$ for $d_{p,VED}$ = 50 nm and ~7 $m^2\ g^{-1}$ for $d_{p,VED}$ = 100 nm. One key reason that differences may exist between studies is that the BC particles sampled had differing maturity. Soot maturity refers to the extent to which the BC has a more disordered internal structure with high hydrogen content (low maturity) versus a more ordered, graphite-like structure with low hydrogen content (high maturity) (Johansson et al., 2017). The absorption cross-section for BC likely increases with increasing soot maturity (López-Yglesias et al., 2014).

The observations are compared with the calculated *MAC* values, based on the fits from Figure 2. *MAC* values from the RDG approximation are independent of *x*, as the particle *MAC* is equal to the *MAC* of the individual spherules making up the particle. Here, the observed *MAC* values in the plateau (large *x*) regime correspond reasonably well with the *MAC*s as calculated from RDG values when the optimal RI values are used. The constant RDG *MAC* value at λ = 532 nm (= 8.8 $m^2\ g^{-1}$) is slightly larger than the often suggested value for atmospheric BC by Bond and Bergstrom (2006) of 7.75 ± 1.2 $m^2\ g^{-1}$ (extrapolated from 7.5 at λ = 550 nm using 1 for the *AAE*) and is identical to that reported for soot from a Santoro-type diffusion burner operating on propane (Zhang et al., 2008). However, the *MAC*s predicted from RDG overestimate the observed *MAC*s at $x < 0.90$, since the RDG fits are weighted by the greater number of data points at $x > 0.9$ where *MAC*s are approximately constant.

Formatted: Font: Not Bold

Deleted: Figure 2

For Mie theory, calculated *MAC* values for highly absorbing substances, such as BC, have a characteristic shape where the *MAC* is constant up to $x \sim 0.2$, increases monotonically by ~40% until $x \sim 0.9$, and then decreases rapidly towards larger *x*. The Mie theory curves calculated here reproduce the observed values at $x < 0.90$ (especially for λ=532 nm and 630 nm), but substantially underestimated *MAC*s at $x > 0.90$. This facilitates understanding of the Mie model underestimate of σ_{abs} at large *x* (Figure 2). Above $x \sim 0.9$ the calculated Mie *MAC* declines with *x* for all wavelengths, but the observations indicate that the *MAC* is constant. Because *x* occurs at smaller $d_{p,VED}$ for shorter wavelengths than for longer wavelengths, the model-measurement difference in both σ_{abs} and *MAC* is more noticeable at 405 nm than it is at 532 nm, which is more noticeable than at 630 nm. This is a consequence of a greater number of the data points at $x > 0.9$ at 405 nm, past the peak in the Mie-calculated *MAC*.

Deleted: Figure 2

Formatted: Font: Not Bold

The reasonable correspondence between the observed and Mie-calculated *MAC* at smaller sizes is, however, somewhat surprising given that Mie assumes spherical particles, yet the particles are not spherical. One potential reason for the observed dependence of the *MAC* on particle size is that the chemical and optical properties of the particles change with size, and the different chemical composition coincidentally improves agreement with Mie theory. For the diffusion flame, changes in the particle size distribution were induced by changing the amount of dilution nitrogen in the sheath flow. This can influence the maturity of the soot and consequently the soot absorption (López-Yglesias et al., 2014). The observed increase in *MAC* with $d_{\mathrm{p,VED}}$ here exhibits some wavelength dependence, which could reflect differences in the sensitivity of the *MAC* to maturation. The observed differences between the *MAC*s observed at the smallest x and the maximum *MAC* values were 21%, 41% and 37% for $\lambda = 405$ nm, $\lambda = 532$ nm and $\lambda = 630$ nm, respectively. However, one additional difference between the wavelengths is that at $\lambda = 405$ nm there is a small increase in *MAC* going from $d_{\mathrm{p,VED}}$ ~60 nm ($x_{405\mathrm{nm}} = 0.6$) to ~100 nm ($x = 0.9$) after which the *MAC* is constant, while at $\lambda = 630$ nm there is much more of a continuous increase in the *MAC* up to larger particle sizes. This could indicate that, at some point, further changes in the soot maturity (composition) have no influence at short wavelengths, but do at longer wavelengths. As a complementary explanation, Dastanpour et al. (2017) observed an increase in primary spherule size with overall particle size for methane diffusion flame generated soot. They attribute the increase in *MAC* with $d_{\mathrm{p,VED}}$ to changes in the internal structure and/or the degree of graphitization that occur with changes in spherule size.

Deleted: ,

Deleted: where maturity refers, in general, to the hydrogen content of the soot and is known to influence

The observation of constant *MAC* values for mature soot ($x > 0.9$ or $d_{\mathrm{p,VED}}$ ~160 nm at $\lambda = 532$ nm) is an important result in the context of how BC is commonly treated in climate models. Most climate models simulate the optical properties of BC using spherical particle Mie theory. The observations indicate that Mie theory will likely underestimate the absorption by BC for particles with $x > 0.9$ because, when the particles are sufficiently absorbing, attenuation of light by the outer layers of the (spherical) causes the mass in the center of the particle to not interact with the electromagnetic field (Bond and Bergstrom, 2006;Kahnert and Devasthale, 2011). This suggests that the RDG approximation, or even an assumption of a constant *MAC*, may provide a more accurate representation of BC absorption than Mie theory in climate models, at least for uncoated BC. This conclusion is independent of soot maturity, as the fall off in the *MAC* with increasing size for Mie theory occurs for all strongly absorbing particles. Although atmospheric BC particles are predominately generated through combustion of fossil fuels or through biomass burning (Bond et al., 2013), flame-generated BC particles have been shown to be a suitable proxy for atmospheric BC particles, both in terms of chemical bonding and structural properties (Slowik et al., 2007;Hopkins et al., 2007). For example, Hopkins et al. (2007) find that the sp^2 content of ethylene and methane flame soot are similar to diesel soot (63%, 60%, and 56%, respectively), and have similar aromatic content. There is also a reasonable similarity between SP-AMS mass spectra of flame soot and soot particles in diesel exhaust or smoke from biomass burning (Onasch et al., 2015a). The absolute values of the derived *RI* may be different for diesel or biomass BC particles, but it can be reasonably assumed that Mie theory does not reproduce the behavior of atmospheric BC particles.

Deleted:

The discrepancy between Mie theory and the observations is both size and wavelength dependent. Consequently, the extent to which the true absorption by BC is underestimated by a given atmospheric model due to inappropriate use of Mie theory will depend importantly on the assumed size distribution, both the position and the width, and the wavelength. Using the effective *RI* values determined here, we estimate that absorption is underestimated by around 20-40% when Mie theory is used with reasonable BC size distributions. The underestimate in absorption from the use of Mie theory will be even larger if non-theory-specific (typically lower) imaginary *RI* values are used, such as that suggested by Hess et al. (1998) or Bond and Bergstrom (2006), as discussed by Stier et al. (2007). Consider that the maximum *MAC* predicted using the Hess et al. (1998) *RI* (=1.75-0.44*i*) from Mie theory is only 3.8 m^2 g^{-1}

5.1.4 MEC and SSA values of nascent and coated-denuded soot

Measurement of b_{ext} and the *MEC* were made in addition to the b_{abs} and *MAC* measurements (Figure 3). Above, the *RI* fitting was performed using only the absorption measurements, in part because calculation of extinction using RDG requires additional assumptions regarding the particle shape. Nonetheless, it is informative to compare the σ_{ext} and *MEC* observations to Mie theory calculations since the overall climate impacts of BC depend on both absorption and scattering. As with the *MAC* values, the observed *MEC* values also increase with x up to 0.90 (or $d_{p,VED}$ up to 160 nm), after which point they are relatively constant (Figure 3). The Mie theory *MEC*s calculated

Formatted: Font: Not Bold

Deleted: Figure 3

Formatted: Font: Not Bold

Deleted: Figure 3

using the *RI*s determined by fitting the absorption measurements (Table 1) agree reasonably well with observations when $x < 0.9$ (using the fits that were constrained to this range), but, as with absorption, Mie theory underestimates the *MEC* above $x = 0.9$. For a given particle size, there is somewhat greater scatter in the observed *MEC*s than in the *MACs*. This is likely a result of the scattering being more sensitive to the shape of the soot particles than is absorption and that the nascent and coated-denuded particle results are combined here.

Deleted: Table 1

Formatted: Font: Not Bold

Given this, the dependence of the *SSA* on particle size is considered separately for the nascent (more lacy) and coated-denuded (more compact) particles. The coated-denuded particle *SSA*s increase with $d_{p,\mathrm{VED}}$, most noticeably for $d_{p,\mathrm{VED}} > 100$ nm, up until $d_{p,\mathrm{VED}} \sim 160$ nm. Above this size the SSA values are approximately constant at a value of ~ 0.30 (Figure 4A). (Results at λ = 532 nm are shown in Figure 4A, but there is a strong correlation between *SSA* at 532 nm and at 405 nm or 630 nm; Figure S5). In contrast, the nascent SSAs increase slightly from $d_{p,\mathrm{VED}}$ ~50 nm to 80 nm, but above 80 nm are approximately constant at ~ 0.20. This demonstrates that particle collapse leads to an increase in the SSA for BC, consistent with Radney et al. (2014). This behavior is also consistent with modelling studies, which have predicted that compact agglomerates exhibit higher SSA values than lacy agglomerates, with an absolute increase of $\Delta SSA \sim 0.1$ (Scarnato et al., 2013) or by a factor of 1.2 – 2.2, depending on the extent of compaction (China et al., 2015a;China et al., 2015b). The increase upon collapse is attributed to the stronger scattering and electromagnetic coupling between spherules in compact aggregates. Here, the difference between the SSA for nascent and coated-denuded soot increases somewhat with particle size, which may result from changes in soot maturity with size. The *SSA*s from this study compare reasonably well to values reported previously at visible wavelengths. For example, Saliba et al. (2016) report *SSA* = 0.16 to 0.26 for nascent soot emitted from a cookstove; Schnaiter et al. (2003);(2006) report *SSA* = 0.2 to 0.3 for soot from a propane diffusion flame, SSA = 0.18 to 0.25 for kerosene-derived soot, and SSA = 0.1 to 0.25 for methane diffusion flame soot; and Sharma et al. (2013) report *SSA* = 0.18 to 0.25 for soot generated from a kerosene lamp. However, the values reported here, are much smaller than the value of 0.5 reported in Radney et al. (2014). The Mie-theory calculated *SSA* values are similar to observations, although show a somewhat stronger increase with size and seem to plateau at larger *SSA* values at large sizes compared to observations.

Deleted: Figure 4

Formatted: Font: Not Bold

Formatted: Font: Not Bold

Deleted: Figure 4

5.1.5 Absorption Ångström Exponent (AAE) of nascent and coated-denuded soot

The wavelength dependence of absorption has been considered by calculating the *AAE* using the measurements at λ = 405 nm and 532 nm (Figure 4B). The nascent *AAE*s at larger particle sizes are slightly larger than the coated-denuded *AAE*s, suggesting that particle collapse leads to a slight decrease in the wavelength dependence of absorption. The average *AAE* was 1.38 ± 0.36 (N = 85) and 1.10 ± 0.37 (N = 135) for nascent and coated-denuded particles, respectively. There is some indication that *AAE* decreases with particle size. This may again be the result of the soot maturity increasing (and the composition changing) with size. The *AAE* values from Mie theory, based on the best-fit *RI* values determined above, exhibit an increase to $x \sim 0.5$ where they peak and then decrease sharply. This predicted decrease is inconsistent with the observations. The *AAE*s calculated using the RDG approximation from the best-fit RI values are constant.

Formatted: Font: Not Bold

Deleted: Figure 4

BC is commonly assumed to have an *AAE* = 1 (Bergstrom, 1973). The measurements here are consistent with this expectation for the collapsed (coated-denuded) particles, but the nascent particles give an *AAE* that is somewhat larger than 1. The observed *AAE* values are similar to results from previous studies examining either freshly emitted soot particles or soot particles containing very little organic material (Schnaiter et al., 2003;Schnaiter et al., 2006;Kirchstetter et al., 2004;Bergstrom et al., 2002;You et al., 2016;Sharma et al., 2013).

5.2 Optical properties of BC from the ethylene flat-burner flames

5.2.1 Results from BC2: Sampling high above the burner surface

During BC2, the ethylene flame was sampled at a height of ~20.3 cm above the surface. At this height, the particles were likely reasonably mature, at least relative to sampling that was performed further into the flame, as was done in BC3+. Particle optical properties were quantified at λ = 405 nm, 532 nm, and 781 nm, with two independent measurements at 532 nm considered (NOAA and PASS-3). As with the methane diffusion flame, the data were fit using Mie theory and the RDG approximation to determine optimal, theory-specific, wavelength-dependent RI values (Table 2). The soot particles from this flame had, overall, a greater amount of intrinsic organic carbon associated with them compared to the particles from the methane diffusion flame. As such, denuding even of the nascent particles led to changes in the optical properties and particle masses.

Deleted: Table 2

Formatted: Font: Not Bold

Thus, the nascent and denuded particles are considered separately, and we focus on the denuded particles. The range of particle sizes considered was also overall smaller than that for the methane diffusion flame.

The retrieval of effective refractive indices for this flame using Mie theory resulted in a good fit to σ_{abs} versus $d_{p,VED}$ for all λ and $d_{p,VED}$ (Figure 5A, D,G, and J, and Figures S6-S7). This difference from the methane diffusion flame is in large part due to the more restricted size range encountered here, with BC particles only up to $d_{p,VED}$ = 160 nm used. The RDG approximation yielded a reasonably good fit across all particle sizes for the ethylene particles, although with some overestimation at smaller sizes. The *MAC* values tended to increase with particle size or size parameter, most obviously at 532 nm where the most data points are available (Figure 5B, E, H, and K). The range of binned *MAC*s shown in Figure 5 are listed in Table S4. The *MAC* values determined using the two PAS instruments at 532 nm differ somewhat, with the NOAA PAS *MAC*s slightly larger than PASS-3 *MAC*s, although the differences are within the measurement uncertainties. Most likely, this instrument difference stems from differences in calibration methods.

Deleted: Figure 5

Formatted: Font: Not Bold

Deleted: Figure 5

Formatted: Font: Not Bold

Formatted: Font: Not Bold

Deleted: Figure 5

The observed *MAC* values tend to be larger for the denuded particles than for the nascent particles, most likely due to less-absorbing organics present in nascent soot that contribute ~25% of the particle mass (Cross et al., 2010). The *MAC* values at λ = 405 nm and 532 nm for the denuded BC2 ethylene flame soot are comparable, within uncertainty, to the *MAC* values for the methane diffusion flame soot for the particles with $d_{p,VED} \sim 150$ nm. This indicates that the BC from these two flames is similarly absorbing in nature.

The impact of particle morphology on the *SSA* and *AAE* is considered by comparing the results for nascent-denuded particles with coated-denuded particles (Figure 6). Nascent particles are excluded because the presence of intrinsic organics can increase *AAE* if the organic material contains brown carbon and can increase the *SSA* independent of the underlying BC morphology. The $D_{f,m}$ values were 2.12 ± 0.06, 2.49 ± 0.07, and 2.17 ± 0.06 for nascent-denuded, sulfuric acid coated-denuded, and DOS coated-denuded soot, respectively (Cross et al., 2010). The nascent-denuded and DOS coated-denuded particles have *SSA* values close to 0, whereas the sulfuric acid coated-denuded

Deleted: Figure 6

Formatted: Font: Not Bold

particles have *SSA* values closer to 0.15 at $x > 0.5$, consistent with particle collapse leading to an increase in *SSA* (Figure 6A). The *SSA* values for the nascent-denuded particles from this flame are smaller than the *SSA* values for the nascent particles from the methane diffusion flame. The reason for this is not clear, but is likely related to differences in the particle shapes and/or the sizes of the spherules; the $D_{\mathrm{f,m}}$ for the nascent-denuded particles here ($D_{\mathrm{f,m}} = 2.12$) is slightly smaller than for the particles from the methane diffusion flame ($D_{\mathrm{f,m}} = 2.28$) (Figure S8). The sulfuric acid coated-denuded particle *SSA* values from the BC2 ethylene flame are also lower than the methane diffusion flame coated-denuded *SSA* values for a given size (Figure 6A), despite having similar $D_{\mathrm{f,m}}$ values.

Deleted: Figure 6

Formatted: Font: Not Bold

Deleted: Figure 6

Formatted: Font: Not Bold

The *AAE* values (using the $\lambda = 405$ nm and 532 nm pair) for nascent-denuded and coated-denuded particles are generally similar when compared over the same size range (Figure 6B). However, the sulfuric acid coated-denuded particle *AAE* values may be slightly smaller than for the nascent-denuded or DOS coated-denuded particles; all are close to unity at $x \sim 0.8$. This indicates that changes in morphology do not lead to substantial changes in *AAE*. The *AAE*s for the coated-denuded particles decrease strongly with $d_{\mathrm{p,VED}}$, with the mean *AAE* ~1.6 for the smallest particles ($x = 0.5$) and *AAE* mean ~ 0.5 for the largest particles ($x = 0.9$). Values below 1 contrast with the methane data, but have been observed in a few previous studies (Clarke et al., 2007;Hadley et al., 2008;Lack et al., 2008). While such a decrease with size is consistent with Mie theory predictions, given the *MAC* results it seems more likely that the size dependence of the *AAE* is related to changes in the soot maturity with particle size. To the extent that the larger particles, which tend to have larger *MAC* values, are reflective of more mature soot this suggests that mature soot from this flame type has an *AAE*<1.

Formatted: Font: Not Bold

Deleted: Figure 6

5.2.2 Results from BC3+: Sampling near the burner surface

During BC3+, the particles were sampled at variable heights above the burner surface to select for particles in different size ranges, but most often they were sampled from relatively close to the burner surface (5.1 cm) compared to BC2 sampling conditions (20.3 cm). It is likely that these different sampling conditions gave rise to particles with different chemical properties. Multiple studies have shown changes in soot maturity and soot optical properties as a function of sampling height in ethylene premixed flames, though at a distance significantly closer to the flame front than sampled here (Olofsson et al., 2015;Migliorini et al., 2011). The particles during BC3+ had very little, if any, intrinsic organic carbon, unlike the BC2 particles that were ~25% organic by mass. However, the small organic content for BC3+ was likely a consequence of the use of a hot sampling line prior to dilution. Consequently, the optical properties of both nascent and denuded ethylene soot particles from BC3+ (sampled close to the burner) differ substantially from the BC2 particles (sampled well above the burner). Average *MAC* values over various size ranges are listed in Table S5. In general, the *MAC*s for BC3+ ethylene particles are similar to BC2 particles at $\lambda = 405$ nm, whereas the $\lambda = 532$ nm *MAC* for BC3+ particles are smaller than those for BC2 particles. (Measurements at $\lambda = 630$ nm were not made during BC2 nor were measurements at 781 nm made during BC3+.) At $d_{\mathrm{p,VED}} > 70$ nm, the $\lambda = 405$ nm *MAC* values were approximately constant with increasing $d_{\mathrm{p,VED}}$ (Figure S9). The behaviour is consistent with methane diffusion flame observations, but the constant *MAC* seems to occur at a lower $d_{\mathrm{p,VED}}$. The number of available data point available for the BC3+ ethylene particles is limited, making conclusions regarding size-dependence of properties somewhat tenuous. The *AAE* for BC3+ ethylene particles are reasonably independent of particle size (Figure S10). The average value of $AAE_{\mathrm{405nm\text{-}532nm}} = 2.01 \pm 0.21$ for $x > 0.5$, which is higher than observed for the methane diffusion flame for this range of x ($=1.18 \pm 0.35$). These observations indicate that differences in sampling and soot maturity result in different optical properties. Previous studies have observed differences in optical properties, chemical composition, and primary spherule size for different flame sampling heights (Bladh et al., 2011;Olofsson et al., 2015;Migliorini et al., 2011). Absorption by less mature soot appears to decrease more rapidly with wavelength than for more mature soot, such that the *MAC* values in the mid-visible (e.g. $\lambda = 532$ nm and 630 nm) are lower for less mature soot. These wavelength-dependent optical results appear to match trends observed previously using active remote sensing techniques to characterize particles within flames (Olofsson et al., 2015;Migliorini et al., 2011). The extent to which this conclusion can be generalized will require further investigation.

6 Conclusion

Light absorption and extinction cross-sections were measured for nascent, denuded, and coated-denuded soot particles that were produced from two different flame types that operated on different fuels (methane or ethylene). These measurements were used in conjunction with particle mass and size measurements to determine various intensive optical properties (e.g. *MAC*, *SSA* and *AAE*) for uncoated BC particles in the size range 50 nm < $d_{\mathrm{p,VED}}$ < 210 nm (corresponding to 0.1 fg < m_p < 5 fg). The optical properties varied somewhat with particle size, most likely due to changes in the chemical nature (i.e. maturity) of the BC that results from variations in the combustion and sampling conditions. However, for larger, mature particles, corresponding to those with $d_{\mathrm{p,VED}}$ > ~160 nm, the observed intensive properties were generally size independent. The observed *MAC* values for BC, measured over multiple studies, are independent of particle collapse and thus provide evidence that absorption by soot of a given maturity level is dictated primarily by the individual spherules and is thus largely size- and shape-independent. The observed *MAC* values are also larger than the recommended value of Bond and Bergstrom (2006), i.e. 8.6 $\mathrm{m^2\ g^{-1}}$ versus 7.75 $\mathrm{m^2\ g^{-1}}$ at 532 nm.

The observations serve as the basis for determination of wavelength- and theory-specific effective complex refractive indices, using both Mie theory and the RDG approximation. With Mie theory, good fits were only obtained for size parameters smaller than ~0.90 (corresponding to $d_{\mathrm{p,VED}}$ ~160 nm for $\lambda = 532$ nm). Above this size, Mie theory predicts a sharp decrease in the *MAC* while the observed *MAC* are constant. Thus, Mie theory systematically under-predicts the observed absorption for $x > 0.9$ and a good fit is not possible. This is because with Mie theory when the particles are sufficiently absorbing and large, light is attenuated by the outer layers of the (spherical) particle such that the mass in the center of the particle does not interact efficiently with the electromagnetic field (Bond and Bergstrom, 2006;Kahnert and Devasthale, 2011).

Our analysis has important implications for the calculation of absorption in atmospheric models. Atmospheric models that use Mie theory, which is the majority, likely underestimate the actual absorption by uncoated BC whether or not theory-specific *RI* values are used; the magnitude of the underestimation will depend on the assumed BC size distributions, increasing with increasing $d_{\mathrm{p,VED}}$ and size distribution width. This may be especially important to consider for simulation of absorption by BC particles from biomass burning, which are larger than those from urban sources (Schwarz et al., 2008). The underestimate of absorption by Mie theory will likely be even larger if non-theory specific RI values that inherently underestimate *MAC* values are used, which includes some of the more commonly used RI values.

Overall, our results demonstrate that either an assumption of a constant *MAC* or the use of the RDG approximation with theory-specific *RI* values (which are equivalent) in atmospheric models are likely to provide for more accurate representation of absolute absorption by uncoated BC than does Mie theory. Further work will be necessary to understand how these results for uncoated BC will impact calculations of absorption by coated BC, for which absorption can be enhanced. However, our results suggest that the absolute absorption by coated particles will be similarly underestimated if core-shell Mie theory is used, regardless of the accuracy of the absorption enhancement calculation.

7 Data Availability

The data associated with this paper are archived at the UC Davis DASH data repository and are available for download from https://doi.org/10.25338/B8JP4V.

8 Acknowledgements

The BC2 study was supported by the US Department of Energy (DOE) grant No. DE-FG02-05ER63995 and the Atmospheric Chemistry Program of the National Science Foundation grants No. ATM-0525355. The BC3 and BC3+ studies were supported by the DOE ASR program grant DE-SC0006980, the EPA STAR Program grant R835033, and the NSF grant ATM-0854916. The BC4 study was supported by DOE grant DE-SC0011935 and the NSF grants AGS-1244918 (Boston College) and AGS-1244999 (Aerodyne), and the participation of the SP2 was made possible by DOE. LANL thanks U.S. Department of Energy's Atmospheric System Research, an Office of Science, Office of Biological and Environmental Research program for funding

Deleted: DOE

9 References

Bergstrom, R. W.: Extinction and absorption coefficients of the atmospheric aerosol as a function of particle size, Contrib. Atmos. Phys., 46, 223-234, 1973.

Bergstrom, R. W., Russell, P. B., and Hignett, P.: Wavelength dependence of the absorption of black carbon particles: Predictions and results from the TARFOX experiment and implications for the aerosol single scattering albedo, Journal of the Atmospheric Sciences, 59, 567-577, 10.1175/1520-0469(2002)059<0567:wdotao>2.0.co;2, 2002.

Bhandari, J., China, S., Onasch, T., Wolff, L., Lambe, A., Davidovits, P., Cross, E., Ahern, A., Olfert, J., Dubey, M., and Mazzoleni, C.: Effect of Thermodenuding on the Structure of Nascent Flame Soot Aggregates, Atmosphere, 8, 166, 10.3390/atmos8090166, 2017.

Bladh, H., Johnsson, J., Olofsson, N. E., Bohlin, A., and Bengtsson, P. E.: Optical soot characterization using two-color laser-induced incandescence (2C-LII) in the soot growth region of a premixed flat flame, Proc. Combust. Inst., 33, 641-648, 10.1016/j.proci.2010.06.166, 2011.

Bohren, C. F., and Huffman, D. R. : Absorption and scattering of light by small particles, Wiley, New York, 1983.

Bond, T. C., and Bergstrom, R. W.: Light Absorption by Carbonaceous Particles: An Investigative Review, Aerosol Science and Technology, 40, 27-67, 10.1080/02786820500421521, 2006.

Bond, T. C., Doherty, S. J., Fahey, D. W., Forster, P. M., Berntsen, T., DeAngelo, B. J., Flanner, M. G., Ghan, S., Kärcher, B., Koch, D., Kinne, S., Kondo, Y., Quinn, P. K., Sarofim, M. C., Schultz, M. G., Schulz, M., Venkataraman, C., Zhang, H., Zhang, S., Bellouin, N., Guttikunda, S. K., Hopke, P. K., Jacobson, M. Z., Kaiser, J. W., Klimont, Z., Lohmann, U., Schwarz, J. P., Shindell, D., Storelvmo, T., Warren, S. G., and Zender, C. S.: Bounding the role of black carbon in the climate system: A scientific assessment, Journal of Geophysical Research: Atmospheres, 118, 5380-5552, 10.1002/jgrd.50171, 2013.

Boucher, O., Randall, D., Artaxo, P., Bretherton, C., Feingold, G., Forster, P., Kerminen, V.-M., Kondo, Y., Liao, H., Lohmann, U., Rasch, P., Satheesh, S. K., Sherwood, S., Stevens, B., and Zhang, X. Y.: Clouds and Aerosols, in: Climate Change 2013: The Physical Science Basis. Contribution of Working Group I to the Fifth Assessment Report of the Intergovernmental Panel on Climate Change, edited by: Stocker, T. F., Qin, D., Plattner, G.-K., Tignor, M., Allen, S. K., Boschung, J., Nauels, A., Xia, Y., Bex, V., and Midgley, P. M., Cambridge University Press, Cambridge, United Kingdom and New York, NY, USA, 571-658, 2013.

Canagaratna, M. R., Jayne, J. T., Jimenez, J. L., Allan, J. D., Alfarra, M. R., Zhang, Q., Onasch, T. B., Drewnick, F., Coe, H., Middlebrook, A., Delia, A., Williams, L. R., Trimborn, A. M., Northway, M. J., DeCarlo, P. F., Kolb, C. E., Davidovits, P., and Worsnop, D. R.: Chemical and microphysical characterization of ambient aerosols with the aerodyne aerosol mass spectrometer, Mass Spectrometry Reviews, 26, 185-222, 10.1002/mas.20115, 2007.

Cappa, C. D., and Wilson, K. R.: Evolution of organic aerosol mass spectra upon heating: implications for OA phase and partitioning behavior, Atmos. Chem. Phys., 11, 1895-2011, 10.5194/acp-11-1895-2011, 2011.

Cappa, C. D., Onasch, T. B., Massoli, P., Worsnop, D. R., Bates, T. S., Cross, E. S., Davidovits, P., Hakala, J., Hayden, K. L., Jobson, B. T., Kolesar, K. R., Lack, D. A., Lerner, B. M., Li, S.-M., Mellon, D., Nuaaman, I., Olfert, J. S., Petäjä, T., Quinn, P. K., Song, C., Subramanian, R., Williams, E. J., and Zaveri, R. A.: Radiative Absorption Enhancements Due to the Mixing State of Atmospheric Black Carbon, Science, 337, 1078-1081, 10.1126/science.1223447, 2012.

China, S., Kulkarni, G., Scarnato, B. V., Sharma, N., Pekour, M., Shilling, J. E., Wilson, J., Zelenyuk, A., Chand, D., and Liu, S.: Morphology of diesel soot residuals from supercooled water droplets and ice crystals: implications for optical properties, Environmental Research Letters, 10, 114010, 10.1088/1748-9326/10/11/114010, 2015a.

China, S., Scarnato, B., Owen, R. C., Zhang, B., Ampadu, M. T., Kumar, S., Dzepina, K., Dziobak, M. P., Fialho, P., Perlinger, J. A., Hueber, J., Helmig, D., Mazzoleni, L. R., and Mazzoleni, C.: Morphology and mixing state of aged soot particles at a remote marine free troposphere site: Implications for optical properties, Geophysical Research Letters, 42, 1243-1250, 10.1002/2014GL062404, 2015b.

Chow, J. C., Watson, J. G., Chen, L.-W. A., Arnott, W. P., Moosmüller, H., and Fung, K.: Equivalence of elemental carbon by thermal/optical reflectance and transmittance with different temperature protocols, Environ. Sci. Technol., 38, 4414-4422, 10.1021/es034936u, 2004.

Clarke, A., McNaughton, C., Kapustin, V., Shinozuka, Y., Howell, S., Dibb, J., Zhou, J., Anderson, B., Brekhovskikh, V., Turner, H., and Pinkerton, M.: Biomass burning and pollution aerosol over North America: Organic components and their influence on spectral optical properties and humidification response, J. Geophys. Res.-Atmos., 112, 10.1029/2006jd007777, 2007.

Cross, E. S., Onasch, T. B., Ahern, A., Wrobel, W., Slowik, J. G., Olfert, J., Lack, D. A., Massoli, P., Cappa, C. D., Schwarz, J. P., Spackman, J. R., Fahey, D. W., Sedlacek, A., Trimborn, A., Jayne, J. T., Freedman, A., Williams, L. R., Ng, N. L., Mazzoleni, C., Dubey, M., Brem, B., Kok, G., Subramanian, R., Freitag, S., Clarke, A., Thornhill, D., Marr, L. C., Kolb, C. E., Worsnop, D. R., and Davidovits, P.: Soot Particle Studies—Instrument Inter-Comparison—Project Overview, Aerosol Science and Technology, 44, 592-611, 10.1080/02786826.2010.482113, 2010.

Dastanpour, R., Momenimovahed, A., Thomson, K., Olfert, J., and Rogak, S.: Variation of the optical properties of soot as a function of particle mass, Carbon, 124, 201-211, 10.1016/j.carbon.2017.07.005, 2017.

Flowers, B. A., Dubey, M. K., Mazzoleni, C., Stone, E. A., Schauer, J. J., Kim, S. W., and Yoon, S. C.: Optical-chemical-microphysical relationships and closure studies for mixed carbonaceous aerosols observed at Jeju Island; 3-laser photoacoustic spectrometer, particle sizing, and filter analysis, Atmos. Chem. Phys., 10, 10387-10398, 10.5194/acp-10-10387-2010, 2010.

Ghazi, R., Tjong, H., Soewono, A., Rogak, S. N., and Olfert, J. S.: Mass, Mobility, Volatility, and Morphology of Soot Particles Generated by a McKenna and Inverted Burner, Aerosol Science and Technology, 47, 395-405, 10.1080/02786826.2012.755259, 2013.

Hadley, O. L., Corrigan, C. E., and Kirchstetter, T. W.: Modified Thermal-Optical Analysis Using Spectral Absorption Selectivity To Distinguish Black Carbon from Pyrolized Organic Carbon, Environmental science & technology, 42, 8459-8464, 10.1021/es800448n, 2008.

Hess, M., Koepke, P., and Schult, I.: Optical Properties of Aerosols and Clouds: The Software Package OPAC, Bulletin of the American Meteorological Society, 79, 831-844, 10.1175/1520-0477(1998)079<0831:opoaac>2.0.co;2, 1998.

Hopkins, R. J., Tivanski, A. V., Marten, B. D., and Gilles, M. K.: Chemical bonding and structure of black carbon reference materials and individual carbonaceous atmospheric aerosols, Journal of Aerosol Science, 38, 573-591, 10.1016/j.jaerosci.2007.03.009, 2007.

Huffman, J. A., Ziemann, P. J., Jayne, J. T., Worsnop, D. R., and Jimenez, J. L.: Development and characterization of a fast-stepping/scanning thermodenuder for chemically-resolved aerosol volatility measurements, Aerosol Sci. Technol., 42, 395-407, 10.1080/02786820802104981, 2008.

Johansson, K. O., El Gabaly, F., Schrader, P. E., Campbell, M. F., and Michelsen, H. A.: Evolution of maturity levels of the particle surface and bulk during soot growth and oxidation in a flame, Aerosol Science and Technology, 51, 1333-1344, 10.1080/02786826.2017.1355047, 2017.

Kahnert, M., and Devasthale, A.: Black carbon fractal morphology and short-wave radiative impact: a modelling study, Atmos. Chem. Phys., 11, 11745-11759, 10.5194/acp-11-11745-2011, 2011.

Khalizov, A. F., Xue, H., Wang, L., Zheng, J., and Zhang, R.: Enhanced Light Absorption and Scattering by Carbon Soot Aerosol Internally Mixed with Sulfuric Acid, Journal of Physical Chemistry A, 113, 1066-1074, 10.1021/jp807531n, 2009.

Kirchstetter, T. W., Novakov, T., and Hobbs, P. V.: Evidence that the spectral dependence of light absorption by aerosols is affected by organic carbon, J. Geophys. Res.-Atmos., 109, 10.1029/2004jd004999, 2004.

Laborde, M., Mertes, P., Zieger, P., Dommen, J., Baltensperger, U., and Gysel, M.: Sensitivity of the Single Particle Soot Photometer to different black carbon types, Atmos. Meas. Tech., 5, 1031-1043, 10.5194/amt-5-1031-2012, 2012.

Lack, D. A., Lovejoy, E. R., Baynard, T., Pettersson, A., and Ravishankara, A. R.: Aerosol absorption measurement using photoacoustic spectroscopy: Sensitivity, calibration, and uncertainty developments, Aerosol Science and Technology, 40, 697-708, 10.1080/02786820600803917, 2006.

Lack, D. A., Cappa, C. D., Covert, D. S., Baynard, T., Massoli, P., Sierau, B., Bates, T. S., Quinn, P. K., Lovejoy, E. R., and Ravishankara, A. R.: Bias in filter-based aerosol light absorption measurements due to organic aerosol loading: Evidence from ambient measurements, Aerosol Science and Technology, 42, 1033-1041, 10.1080/02786820802389277, 2008.

Lack, D. A., Richardson, M. S., Law, D., Langridge, J. M., Cappa, C. D., McLaughlin, R. J., and Murphy, D. M.: Aircraft Instrument for Comprehensive Characterization of Aerosol Optical Properties, Part 2: Black and Brown Carbon Absorption and Absorption Enhancement Measured with Photo Acoustic Spectroscopy, Aerosol Science and Technology, 46, 555-568, 10.1080/02786826.2011.645955, 2011.

Lambe, A., Ahern, A., Williams, L., Slowik, J., Wong, J., Abbatt, J., Brune, W., Ng, N., Wright, J., and Croasdale, D.: Characterization of aerosol photooxidation flow reactors: heterogeneous oxidation, secondary organic aerosol formation and cloud condensation nuclei activity measurements, Atmospheric Measurement Techniques, 4, 445-461, 10.5194/amt-4-445-2011, 2011.

Langridge, J. M., Richardson, M. S., Lack, D., Law, D., and Murphy, D. M.: Aircraft Instrument for Comprehensive Characterization of Aerosol Optical Properties, Part I: Wavelength-Dependent Optical Extinction and Its Relative Humidity Dependence Measured Using Cavity Ringdown Spectroscopy, Aerosol Science and Technology, 45, 1305-1318, 10.1080/02786826.2011.592745, 2011.

Lohmann, U., and Feichter, J.: Global indirect aerosol effects: a review, Atmos. Chem. Phys., 5, 715-737, 10.5194/acp-5-715-2005, 2005.

López-Yglesias, X., Schrader, P. E., and Michelsen, H. A.: Soot maturity and absorption cross sections, Journal of Aerosol Science, 75, 43-64, 10.1016/j.jaerosci.2014.04.011, 2014.

Mackowski, D. W., and Mishchenko, M. I.: Calculation of the T matrix and the scattering matrix for ensembles of spheres, Journal of the Optical Society of America a-Optics Image Science and Vision, 13, 2266-2278, 10.1364/josaa.13.002266, 1996.

Massoli, P., Kebabian, P. L., Onasch, T. B., Hills, F. B., and Freedman, A.: Aerosol Light Extinction Measurements by Cavity Attenuated Phase Shift (CAPS) Spectroscopy: Laboratory Validation and Field Deployment of a Compact Aerosol Particle Extinction Monitor, Aerosol Science and Technology, 44, 428-435, 10.1080/02786821003716599, 2010.

Medalia, A. I., and Heckman, F. A.: Morphology of aggregates—II. Size and shape factors of carbon black aggregates from electron microscopy, Carbon, 7, 567-582, 10.1016/0008-6223(69)90029-3, 1969.

Migliorini, F., Thomson, K., and Smallwood, G.: Investigation of optical properties of aging soot, Applied Physics B: Lasers and Optics, 104, 273-283, 10.1007/s00340-011-4396-4, 2011.

Mullins, J., and Williams, A.: The optical properties of soot: a comparison between experimental and theoretical values, Fuel, 66, 277-280, 10.1016/0016-2361(87)90255-9, 1987.

Olofsson, N.-E., Simonsson, J., Török, S., Bladh, H., and Bengtsson, P.-E.: Evolution of properties for aging soot in premixed flat flames studied by laser-induced incandescence and elastic light scattering, Applied Physics B, 119, 669-683, 10.1007/s00340-015-6067-3, 2015.

Onasch, T. B., Trimborn, A., Fortner, E. C., Jayne, J. T., Kok, G. L., Williams, L. R., Davidovits, P., and Worsnop, D. R.: Soot Particle Aerosol Mass Spectrometer: Development, Validation, and Initial Application, Aerosol Science and Technology, 46, 804-817, 10.1080/02786826.2012.663948, 2012.

Onasch, T. B., Fortner, E. C., Trimborn, A. M., Lambe, A. T., Tiwari, A. J., Marr, L. C., Corbin, J. C., Mensah, A. A., Williams, L. R., Davidovits, P., and Worsnop, D. R.: Investigations of SP-AMS Carbon Ion Distributions as a Function of Refractory Black Carbon Particle Type, Aerosol Science and Technology, 49, 409-422, 10.1080/02786826.2015.1039959, 2015a.

Onasch, T. B., Massoli, P., Kebabian, P. L., Hills, F. B., Bacon, F. W., and Freedman, A.: Single Scattering Albedo Monitor for Airborne Particulates, Aerosol Science and Technology, 49, 267-279, 10.1080/02786826.2015.1022248, 2015b.

Park, K., Cao, F., Kittelson, D. B., and McMurry, P. H.: Relationship between Particle Mass and Mobility for Diesel Exhaust Particles, Environmental Science & Technology, 37, 577-583, 10.1021/es025960v, 2003.

Purcell, E. M., and Pennypacker, C. R.: Scattering and absorption of light by nonspherical dielectric grains, The Astrophysical Journal, 186, 705-714, 10.1086/152538, 1973.

Radney, J. G., You, R., Ma, X., Conny, J. M., Zachariah, M. R., Hodges, J. T., and Zangmeister, C. D.: Dependence of Soot Optical Properties on Particle Morphology: Measurements and Model Comparisons, Environmental science & technology, 48, 3169-3176, 10.1021/es4041804, 2014.

Ramanathan, V., and Carmichael, G.: Global and regional climate changes due to black carbon, Nature Geosci, 1, 221-227, 10.1038/ngeo156, 2008.

Saliba, G., Subramanian, R., Saleh, R., Ahern, A. T., Lipsky, E. M., Tasoglou, A., Sullivan, R. C., Bhandari, J., Mazzoleni, C., and Robinson, A. L.: Optical properties of black carbon in cookstove emissions coated with secondary organic aerosols: Measurements and modeling, Aerosol Science and Technology, 50, 1264-1276, 10.1080/02786826.2016.1225947, 2016.

Scarnato, B. V., Vahidinia, S., Richard, D. T., and Kirchstetter, T. W.: Effects of internal mixing and aggregate morphology on optical properties of black carbon using a discrete dipole approximation model, Atmos. Chem. Phys., 13, 5089-5101, 10.5194/acp-13-5089-2013, 2013.

Schnaiter, M., Horvath, H., Mohler, O., Naumann, K. H., Saathoff, H., and Schock, O. W.: UV-VIS-NIR spectral optical properties of soot and soot-containing aerosols, Journal of Aerosol Science, 34, 1421-1444, 10.1016/s0021-8502(03)00361-6, 2003.

Schnaiter, M., Gimmler, M., Llamas, I., Linke, C., Jaeger, C., and Mutschke, H.: Strong spectral dependence of light absorption by organic carbon particles formed by propane combustion, Atmospheric Chemistry and Physics, 6, 2981-2990, 10.5194/acp-6-2981-2006, 2006.

Schwarz, J. P., Gao, R. S., Spackman, J. R., Watts, L. A., Thomson, D. S., Fahey, D. W., Ryerson, T. B., Peischl, J., Holloway, J. S., Trainer, M., Frost, G. J., Baynard, T., Lack, D. A., de Gouw, J. A., Warneke, C., and Del Negro, L. A.: Measurement of the mixing state, mass, and optical size of individual black carbon particles in urban and biomass burning emissions, Geophysical Research Letters, 35, L13810, 10.1029/2008GL033968, 2008.

Sharma, N., Arnold, I. J., Moosmüller, H., Arnott, W. P., and Mazzoleni, C.: Photoacoustic and nephelometric spectroscopy of aerosol optical properties with a supercontinuum light source, Atmos. Meas. Tech., 6, 3501-3513, 10.5194/amt-6-3501-2013, 2013.

Slowik, J. G., Cross, E. S., Han, J.-H., Davidovits, P., Onasch, T. B., Jayne, J. T., WilliamS, L. R., Canagaratna, M. R., Worsnop, D. R., Chakrabarty, R. K., Moosmueller, H., Arnott, W. P., Schwarz, J. P., Gao, R.-S., Fahey, D. W., Kok, G. L., and Petzold, A.: An inter-comparison of instruments measuring black carbon content of soot particles, Aerosol Science and Technology, 41, 295-314, 10.1080/02786820701197078, 2007.

Sorensen, C. M.: Light Scattering by Fractal Aggregates: A Review, Aerosol Science and Technology, 35, 648-687, 10.1080/02786820117868, 2001.

Sorensen, C. M.: The Mobility of Fractal Aggregates: A Review, Aerosol Science and Technology, 45, 765-779, 10.1080/02786826.2011.560909, 2011.

Stier, P., Seinfeld, J. H., Kinne, S., and Boucher, O.: Aerosol absorption and radiative forcing, Atmos. Chem. Phys., 7, 5237-5261, 10.5194/acp-7-5237-2007, 2007.

Stipe, C. B., Higgins, B. S., Lucas, D., Koshland, C. P., and Sawyer, R. F.: Inverted co-flow diffusion flame for producing soot, Review of Scientific Instruments, 76, 10.1063/1.1851492, 2005.

Wang, R., Balkanski, Y., Boucher, O., Ciais, P., Schuster, G. L., Chevallier, F., Samset, B. H., Liu, J., Piao, S., Valari, M., and Tao, S.: Estimation of global black carbon direct radiative forcing and its uncertainty constrained by observations, Journal of Geophysical Research: Atmospheres, 121, 5948-5971, doi:10.1002/2015JD024326, 2016.

Wu, J.-S., Krishnan, S., and Faeth, G.: Refractive indices at visible wavelengths of soot emitted from buoyant turbulent diffusion flames, Journal of heat transfer, 119, 230-237, 10.1115/1.2824213, 1997.

You, R., Radney, J. G., Zachariah, M. R., and Zangmeister, C. D.: Measured Wavelength-Dependent Absorption Enhancement of Internally Mixed Black Carbon with Absorbing and Nonabsorbing Materials, Environmental Science & Technology, 50, 7982-7990, 10.1021/acs.est.6b01473, 2016.

Zhang, R., Khalizov, A. F., Pagels, J., Zhang, D., Xue, H., and McMurry, P. H.: Variability in morphology, hygroscopicity, and optical properties of soot aerosols during atmospheric processing, Proceedings of the National Academy of Sciences of the United States of America, 105, 10291-10296, 10.1073/pnas.0804860105, 2008.

10 Tables and Figures

Table 1. Refractive indices for methane diffusion flame soot retrieved via fitting Mie Theory and the RDG approximation to the σ_{abs} observations. Nascent and denuded data are combined (see text for details).

Study	Method	λ (nm)	Instrument	$n = m + ki$	MAC_{peak} (m^2/g)	$dp_{\text{VED, peak}}$ (nm) /Size Param.$^{@}$	Number of data points
BC3(+), BC4	Mie$^{\%}$	405	UCD CRD-PAS	1.29 + 1.29i$^{\#}$	18.72 (±6.57)$^{\#}$	61/0.47	225
BC3(+), BC4	Mie$_{x<0.9}$	405	UCD CRD-PAS	2.31 + 1.26i	12.21 (±2.18)	108/0.84	40
BC3(+), BC4	RDG$^{\$,*}$	405	UCD CRD-PAS	1.80 + 1.39i	11.91 (±1.97)		225
BC3(+), BC4	Mie	532	UCD CRD-PAS	2.24 + 1.19i$^{\#}$	9.13 (±3.03)$^{\#}$	142/0.84	219
BC3(+), BC4	Mie$_{x<0.9}$	532	UCD CRD-PAS	1.96 + 1.01i	8.68 (±1.08)	137/0.82	82
BC3(+), BC4	RDG	532	UCD CRD-PAS	1.80 + 1.43i	8.81 (±1.46)		219
BC3(+), BC4	Mie	630	Aerodyne CAPS	2.14 + 0.94i$^{\#}$	6.93 (±0.20)$^{\#}$	181/0.90	169
BC3(+), BC4	Mie$_{x<0.9}$	630	Aerodyne CAPS	2.01 + 0.89i	6.73 (±0.24)	177/0.88	134
BC3(+), BC4	RDG	630	Aerodyne CAPS	1.80 + 1.13i	6.51 (±1.26)		169

[%] Uncertainties in the *MAC* are 1σ from the reduced χ^2 fit. See supplementary figures S3 and S4.

[$] The *n* values from the RDG method are non-unique. Therefore, uncertainty estimates from this work are not available. See text for details.

[@] VED and the size parameter ($x = \pi d_p/\lambda$) where the peak *MAC* occurs

[*] There are many degenerate RI combinations that give similar quality fit to RDG theory. Thus, a value of 1.80 was chosen for the effective real refractive index.

[#] These values are given for reference purposes only, but should not be used due to inability to fit data well (see text for details).

Table 2. Theory-specific effective refractive indices for ethylene premixed flame soot from BC2 and BC3+ retrieved via fitting Mie Theory and the RDG approximation to the σ_{abs} observations. Nascent and denuded experiments are considered separately.

Study[#]	Soot Type	Method	λ (nm)	Instrument	$n = m + ki$	MAC_{peak} (m^2/g)	$dp_{VED, peak}$ (nm) /Size Param.[@]	No. of data points
BC2	Nascent	Mie[%]	405	PASS-3	2.21 + 0.86i	10.45 (±2.06)	123/0.95	36
BC2	Denuded	Mie	405	PASS-3	2.19 + 0.91i	10.68 (±1.97)	119/0.92	30
BC2	Nascent	RDG[$,*]	405	PASS-3	1.80 + 1.13i	10.06 (±2.22)		36
BC2	Denuded	RDG	405	PASS-3	1.80 + 1.18i	10.32 (±2.56)		30
BC2	Nascent	Mie	532	PASS-3	2.13 + 0.64i	6.92 (±0.78)	178/1.07	36
BC2	Nascent	Mie	532	NOAA CRD-PAS	2.39 + 0.79i	8.02 (±0.13)	169/0.99	43
BC2	Denuded	Mie	532	PASS3	1.96 + 0.83i	7.70 (±0.90)	150/0.89	31
BC2	Denuded	Mie	532	NOAA CRD-PAS	2.56 + 1.11i	9.00 (±0.80)	152/0.90	46
BC2	Nascent	RDG	532	PASS-3	1.80 + 0.78i	6.92 (±0.43)		36
BC2	Nascent	RDG	532	NOAA CRD-PAS	1.80 + 0.85i	6.16 (±1.75)		43
BC2	Denuded	RDG	532	PASS-3	1.80 + 1.08i	7.35 (±1.69)		31
BC2	Denuded	RDG	532	CRD-PAS	1.80 + 1.13i	7.55 (±0.68)		46
BC2	Nascent	Mie	781	PASS-3	2.16 + 0.76i	5.10 (±0.40)	250/0.96	31
BC2	Denuded	Mie	781	PASS-3	2.84 + 0.74i	6.20 (±0.20)	239/0.95	36
BC2	Nascent	RDG	781	PASS-3	1.80 + 0.50i	2.59 (±0.33)		36
BC2	Denuded	RDG	781	PASS-3	1.80 + 0.73i	3.64 (±0.81)		31
BC3+	Denuded	Mie	405	UCD CRD-PAS	2.11 + 1.03i	11.09 (±2.82)	110/0.85	27
BC3+	Denuded	RDG	405	UCD CRD-PAS	1.80 + 2.05i	10.78 (±3.11)		27
BC3+	Denuded	Mie	532	UCD CRD-PAS	1.46 + 0.54i	6.03 (±1.12)	118/0.70	22
BC3+	Denuded	RDG	532	UCD CRD-PAS	1.80 + 0.76i	5.61 (±0.46)		22
BC3+	Denuded	Mie	630	CAPS PM_{SSA}	1.78+0.45i	3.93 (±0.90)	188/0.93	22
BC3+	Denuded	RDG	630	CAPS PM_{SSA}	1.80 + 0.55i	3.51 (±1.55)		22

[%] Uncertainties in *MACs* are 1σ from the least χ^2 fit. See Supplementary Figures S7-8.

[$] The *n* values from the RDG method are non-unique. Therefore, uncertainty estimates from this work are not available. See text for details.

[@] VED and the size parameter ($x = \pi d_p/\lambda$) where the peak *MAC* occurs

[*] There are many degenerate RI combinations that give similar quality fit to RDG theory. Thus, a value of 1.80 was chosen for the effective real refractive index.

[#] In BC2 the ethylene flat-burner flame was sampled 20.3 cm between the burner surface and the sampling inlet and during BC3 the flame was sampled 2” between the burner surface and the sampling inlet.

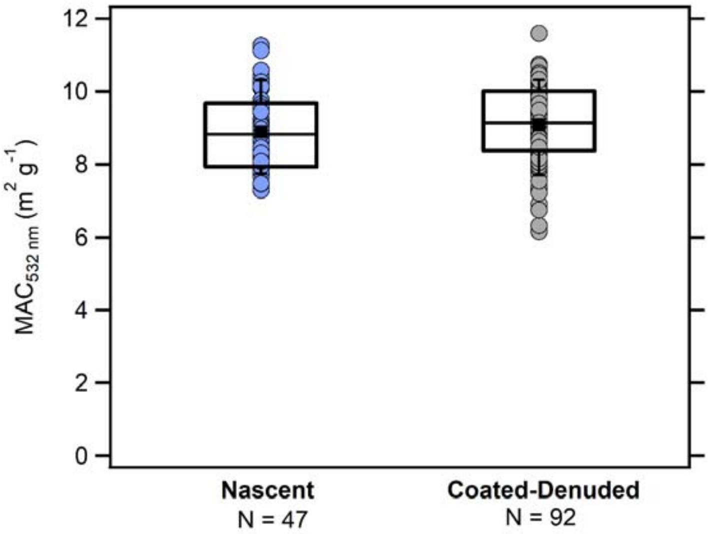

Figure 1. A comparison of methane diffusion-flame generated nascent (or nascent denuded; blue circles) and coated-denuded (grey circles) mass absorption coefficients (*MACs*) at $\lambda = 532$ nm for $x > 0.90$ for BC3, BC3+, and BC4 experiments. Note that conditioning (and therefore the shape) of the soot does not affect the observed *MACs*. The box and whisker plots show the mean (■), median (-), lower and upper quartile (boxes) and 9th and 91st percentile (whisker).

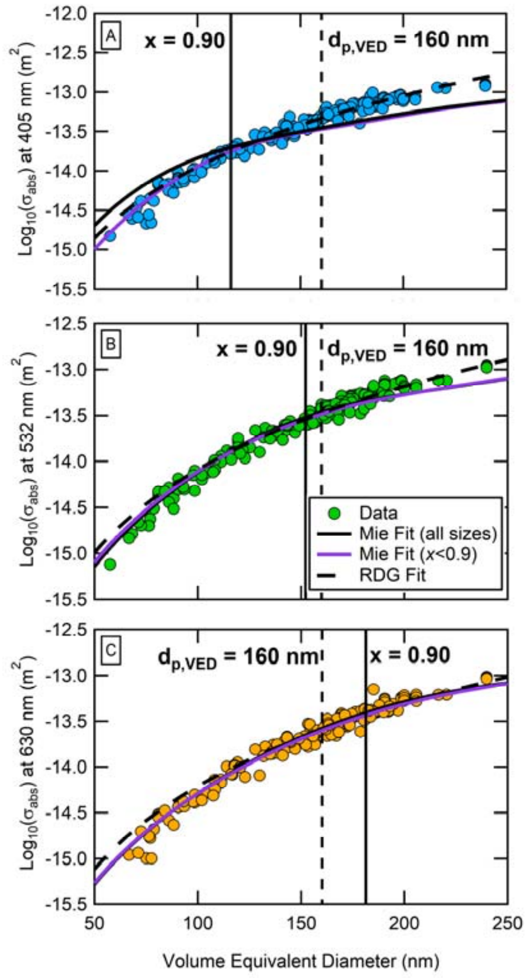

Figure 2. Observed σ_{abs} versus $d_{p,VED}$ methane soot data from BC3,BC3+, and BC4. Panels A and B are λ = 405 nm and 532 nm data, respectively, from the UCD CRD-PAS and panel C is λ = 630 nm data from the CAPS PM_{SSA}. The nascent and coated-denuded data have been combined since there is no significant difference in the absorption cross-sections and *MAC*s between the two datasets. Note the inability of Mie Theory to reproduce the observed $\sigma_{abs,405nm}$ for all sizes. Vertical solid lines indicating x = 0.9, where observations deviate from Mie theory, are provided for reference. In addition, vertical dashed lines indicate $d_{p,VED}$ = 160 nm, above which soot maturity is approximately constant.

Deleted:

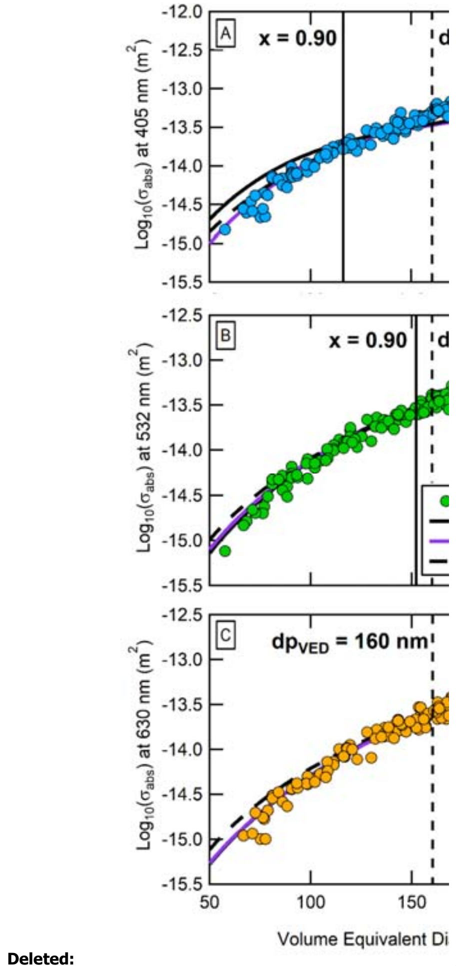

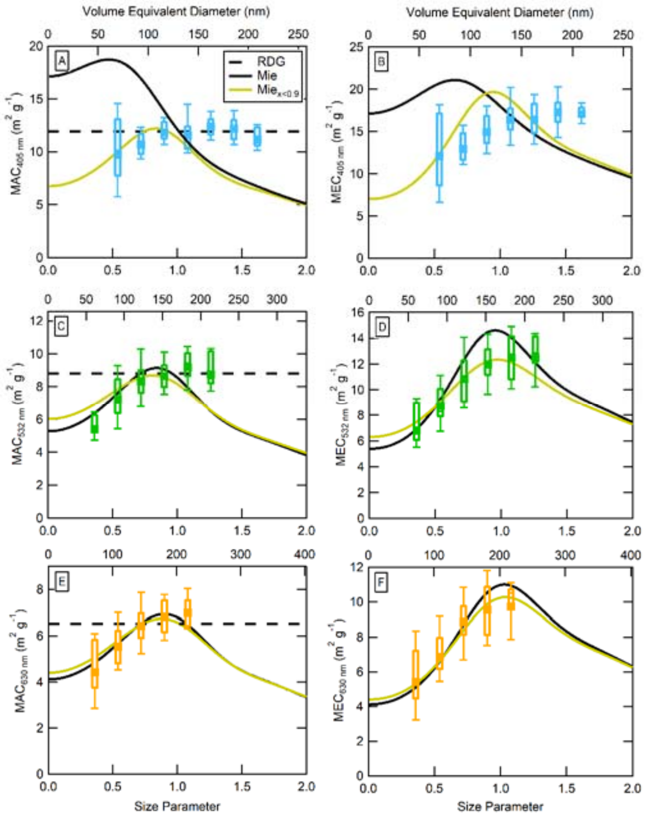

Figure 3. Box plots of *MAC*s and *MEC*s as a function of size parameter, with $\Delta x = 0.18$. The volume equivalent diameters are provided at the top of the plots for reference. Also shown are Mie theory curves for all particles (black solid lines), Mie theory curves for $x < 0.90$ (gold line), and RDG curves (dashed line) calculated from the RI values in Table 1. *RI* fitting was performed using only the absorption measurements. Panels A and B are $\lambda = 405$ nm data from the UCD CRD-PAS, panels C and D are $\lambda = 532$ nm data from the UCD CRD-PAS, and panels E and F are $\lambda = 630$ nm data from the CAPS PM$_{SSA}$. The poor match between the calculated Mie theory curves at $\lambda = 405$ nm reflects the difficulties in fitting spherical particle Mie theory to the observed $\sigma_{abs,405nm}$ over the entire size range. Although the same particle sizes were sampled over all wavelengths, the size parameters sampled at each wavelength are different. Therefore, there are different numbers of boxes for each wavelength. Note that this figure is directly related to Figure 2, the difference being that the y-axis values in Figure 2 (cross-sections) have been divided by the per particle mass to give the *MAC* or *MEC*. Points in each bin range from N=10 at $x_{1.62}$ to N = 81 at $x_{1.26}$ for $\lambda = 405$ nm, N = 5 at $x_{0.36}$ to N = 82 at $x_{1.08}$ at $\lambda = 532$ nm, and N=8 at $x_{1.08}$ to N=67 at $x_{0.9}$ at $\lambda = 630$ nm.

Deleted: Table 1

Formatted: Font: Not Bold

Deleted: Figure 2

Formatted: Font: Not Bold

Formatted: Font: Not Bold

Deleted: Figure 2

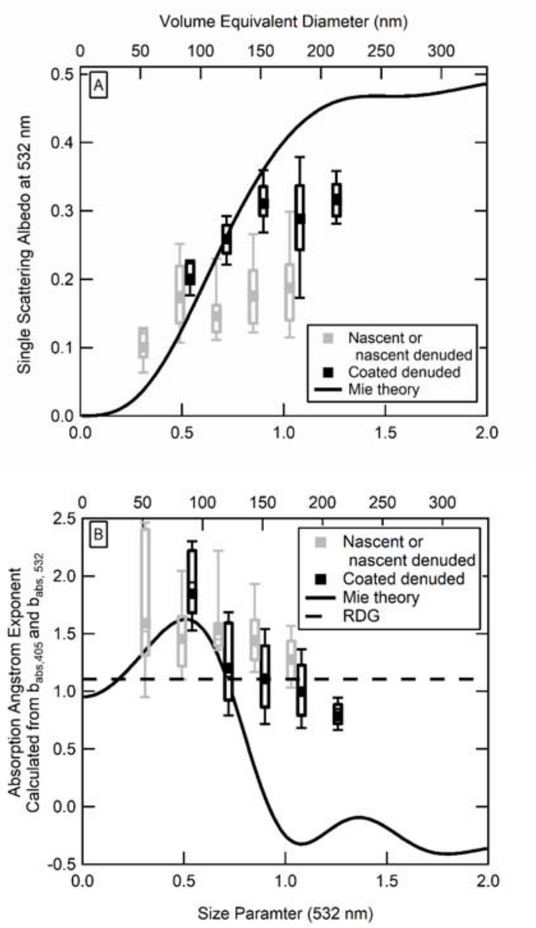

Figure 4. Box and whisker plots of λ = 532 nm (A) single scattering albedo (*SSA*) and (B) absorption Ångström exponent (*AAE*) as a function of volume equivalent diameter produced from the methane diffusion flame. The black points are coated-denuded data (coating material is evaporated following coating with DOS or sulfuric acid) and are potentially collapsed due to coating and the grey points are nascent or nascent denuded data. The black lines are the *SSA* or *AAE* predicted by spherical particle Mie theory and the dashed black line in panel B is *AAE* predicted from the RDG approximation using the effective refractive indices listed in Table 1. The nascent or nascent denuded boxes (black) are shifted by X = 0.05. Points in each bin range from N=6 at $x_{0.36}$ to N = 26 at $x_{1.08}$ for nascent (or nascent denuded) and N=5 at $x_{0.54}$ to N = 9 at $x_{1.26}$ for coated-denuded points.

Formatted: Font: Not Bold

Deleted: Table 1

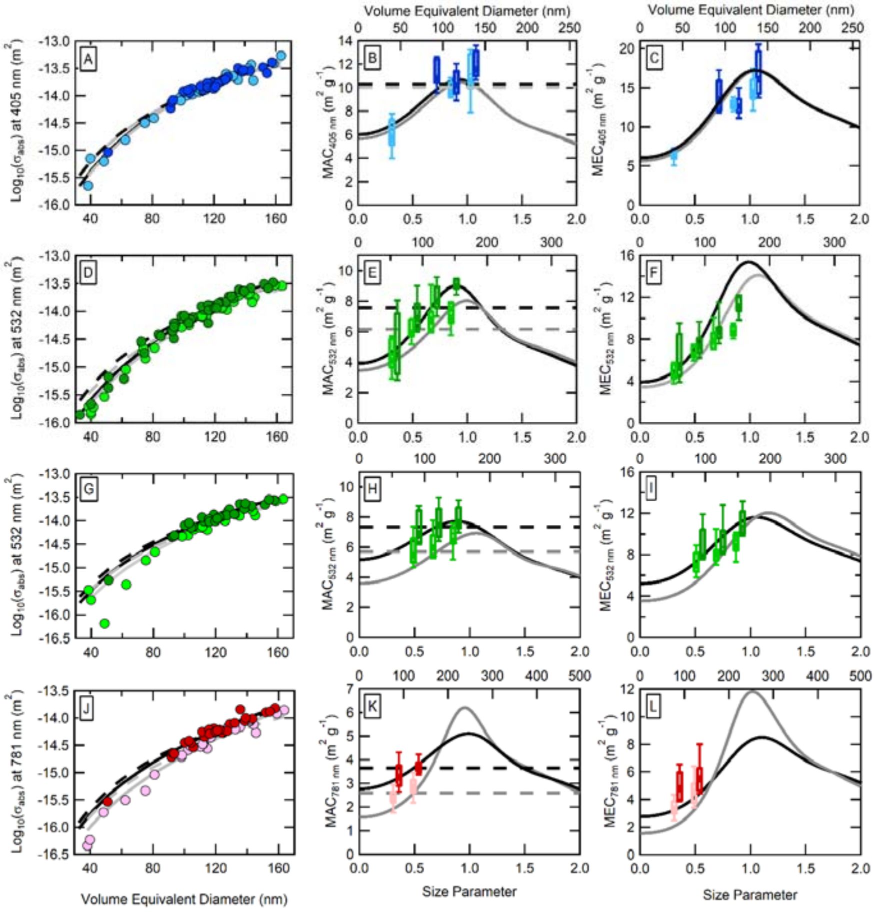

Figure 5. Measured absorption cross-sections vs. volume equivalent diameter (panels in the first column) and mass absorption and extinction coefficients (*MAC*s and *MEC*s; panels in the second and third column, respectively) for ethylene soot sampled 20.3 cm from burner surface of the McKenna flame as a function of size parameter ($x = \pi d_p/\lambda$) (bottom axes) and volume equivalent diameter (top axes). for BC2. Panels A, B, and C show PASS-3 data at λ = 405 nm, panels D, E, F show NOAA PAS data at λ = 532 nm, panels G, H, I show PASS-3 data at λ = 532 nm, and panels J, K, and L show PASS-3 data at λ = 781 nm. The dashed black and grey lines are the RDG fits to denuded and nascent data, respectively, and the solid black and grey lines are Mie fits to denuded and nascent data, respectively.

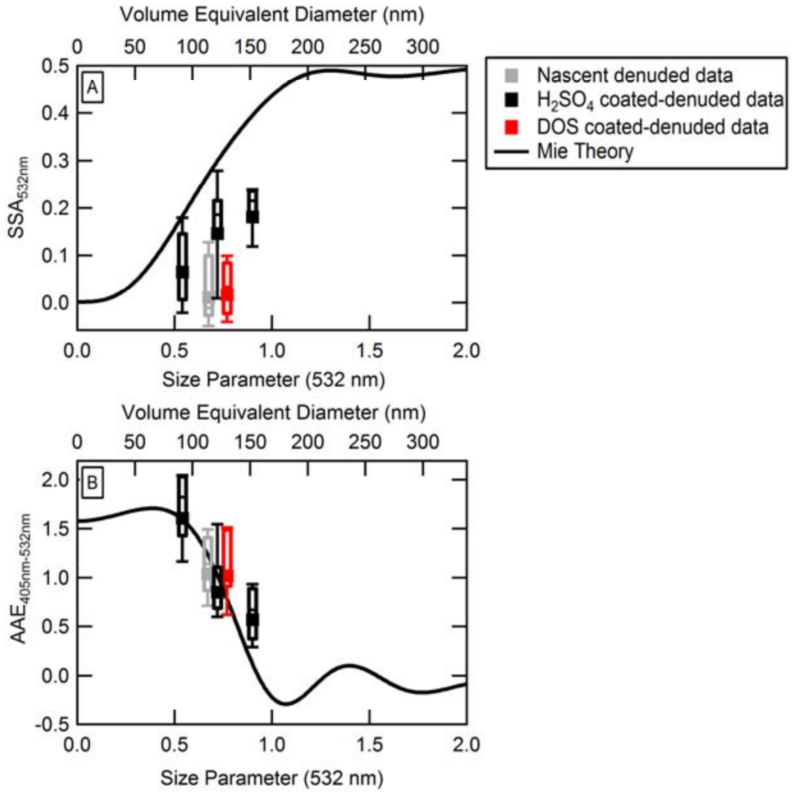

Figure 6. Box and whisker plots of (A) single scattering albedo (*SSA*) and (B) absorption Ångström exponent (*AAE*) as a function of size parameter and volume equivalent diameter produced from the ethylene flame during BC2. The *SSA* was calculated using data from the NOAA PAS and the *AAE* was calculated using data from the λ = 405 nm PASS-3 and the λ = 532 nm NOAA PAS data. The black points are coated-denuded data (coating material is evaporated following coating with DOS or sulfuric acid) and are potentially collapsed due to coating and the gray points are nascent denuded points (evaporation of intrinsic organic matter produced from the ethylene flame). The black lines are the *SSA*s predicted using spherical particle Mie theory using the effective complex refractive index retrieved from fitting the $\sigma_{abs,532nm}$ from the NOAA PAS. Here points are binned with a constant $\Delta x = 0.18$ for the purpose of comparison between the different particle treatments. N = 6 for nascent or nascent denuded points, N=5 for DOS coated-denuded points, and $N_{x=0.54} = 11$, $N_{x=0.72} = 8$, and $N_{x=0.9} = 5$ for H_2SO_4 coated-denuded points.

Supplementary Material for "Measurement and modeling of the multi-wavelength optical properties of uncoated flame-generated soot"

Sara D. Forestieri,[1,#] Taylor M. Helgestad[1,#] Andrew Lambe,[2,3] Lindsay Renbaum-Wolff[2], Daniel A. Lack,[4,5,^] Paola Massoli,[2] Eben S. Cross,[6,&] Manvendra K. Dubey,[7] Claudio Mazzoleni,[8] Jason Olfert,[9] Arthur Sedlacek,[10] Andrew Freedman,[2] Paul Davidovits,[3] Timothy B. Onasch,[2,3] Christopher D. Cappa[1]

[1]Department of Civil and Environmental Engineering, University of California, Davis, CA 95616
[2]Aerodyne Research Inc., Billerica, Massachusetts, USA, 01821
[3]Chemistry Department, Boston College, Boston, MA, USA, 02467
[4]NOAA Earth System Research Laboratory, Boulder, CO, USA, 80305
[5]University of Colorado, Cooperative Institute for Research of the Environmental Sciences, Boulder, CO, USA, 80305
[6]Department of Civil and Environmental Engineering, Massachusetts Institute of Technology, Cambridge, Massachusetts, USA
[7]Los Alamos National Laboratory, Los Alamos, NM, USA
[8]Deparment of Physics and Atmospheric Sciences Program, Michigan Technological University, Houghton, MI, USA
[9]Department of Mechanical Engineering, University of Alberta, Edmonton, Alberta, Canada
[10]Biological, Environmental and Climate Sciences Department, Brookhaven National Laboratory, Upton, New York, USA
[#] Now at: California Air Resources Board, Sacramento, CA, USA
[^] Now at: Transport Emissions, Air Quality and Climate Consulting, Brisbane, Australia
[&] Now at: Aerodyne Research Inc., Billerica, Massachusetts, USA, 01821

Correspondence to: Sara Forestieri (*sara.forestieri@arb.ca.gov*) or Christopher Cappa (cdcappa@ucdavis.edu)

The supplementary material consists of five tables and ten figures.

Formatted: Line spacing: Multiple 1.15 li

Formatted: German (Germany)

Table S1. Summary of terminology

Terminology	*Definition*
Nascent soot	Soot particles that were not subject to additional thermal or chemical processing
Nascent-denuded soot	Soot particles that were heated to 270 °C for ~5 seconds in a thermal denuder
Coated-denuded soot	Soot particles that were first coated with either DOS, H_2SO_4 or SOA and subsequently heated to 270 °C for ~5 seconds in a thermal denuder
Forward-coating experiment	Experiments in which the particles were size selected, then the monodisperse particles were coated, and finally thermally denuded
Reverse-coating experiment	Experiments in which the polydisperse particle distribution was first coated, then the particles were size selected, and finally thermally denuded

Table S2. Summary of instrumentation used in BC2, BC3, BC3+, and BC4.

Instrument	**Manufacturer**	**Measurement**	**Study**
Centrifugal particle mass analyzer (CPMA)	Cambustion	Per particle mass in fg particle^{-1}	All Studies
Scanning mobility particle sizer (SMPS)	TSI	Particle mobility size distributions	All Studies
Condensation particle counter (CPC)	TSI	Number concentration of particles in particles cm^{-3}	All Studies
3 wavelength photoacoustic soot spectrometer (PASS-3) equipped with scattering sensor	Droplet Measurement Technologies	Aerosol absorption and extinction coefficients (b_{abs} and b_{ext}) at λ = 405 nm, 532 nm, and 781 nm in Mm^{-1}	BC2
NOAA photoacoustic spectrometer (PAS)	Custom-built	b_{ext} at λ = 532 nm in Mm^{-1}	BC2
NOAA cavity ringdown spectrometer (CRD)	Custom-built	b_{abs} at λ = 532 nm in Mm^{-1}	BC2
UC Davis CRD-PAS	Custom-built	b_{abs} and b_{ext} in Mm^{-1} at λ = 405 nm and 532 nm	BC3, BC3+, and BC4
Cavity attenuated phase shift single scatter albedo spectrometer (CAPS PM_{SSA})	Aerodyne Research	Scattering and absorption coefficients (b_{sca} and b_{ext}) in Mm^{-1} at λ = 630 nm	BC3, BC3+, and BC4
Soot particle aerosol mass spectrometer (SP-AMS)	Aerodyne Research	Chemical and physical properties of black carbon	BC2, BC3, and BC4
Compact time-of-flight aerosol mass spectrometer (c-ToF-AMS)	Aerodyne Research	Chemical composition of non-refractory aerosol	BC3

Table S3. Observed mean *MAC*s for the methane flame, averaged across BC3, BC3+ and BC4. Uncertainties are reported as 1σ standard deviations over the measurements

λ (nm)	*MAC* (m^2 g^{-1}) (all points)	*AAE*	*MAC* (m^2 g^{-1}) ($x > 0.9$)	*AAE*	*MAC* (m^2 g^{-1}) ($x < 0.9$)	*AAE*
405	11.8 ± 1.7	1.16^*	12.1 ± 1.4	1.04	11.1 ± 2.0	1.20
532	8.6 ± 1.3	$1.42^\#$	9.1 ± 1.1	1.21	8.0 ± 1.4	1.35
630	6.3 ± 1.2	1.84^+	7.1 ± 1.1	1.47	6.1 ± 1.2	1.60

* 405-532 nm; $^\#$ 405-630 nm; $^+$ 532-630 nm

Table S4. Minimum and maximum binned *MAC*s for all flame types.

		Smallest *x* bin			**Largest *x* bin**		
λ (nm)	**Instrument**	**Size parameter**	**# Data Points**	***MAC*** (m^2 g^{-1})	**Size parameter**	**# Data Points**	***MAC*** (m^2 g^{-1})
		Methane Diffusion Flame (BC3, BC3+ & BC4)					
405	UCD CRD-PAS	0.54	13	9.7 ± 3.2	1.62	10	11.2 ± 1.0
532	UCD CRD-PAS	0.36	5	5.4 ± 0.8	1.26	11	8.7± 1.0
630	CAPS PM_{SSA}	0.36	14	4.4 ± 0.8	1.08	8	7±0.67
		Ethylene Premixed Flame Denuded (BC2)					
405	PASS-3	0.72	7	10.8± 1.5	1.08	5	11.5±1.3
532	PASS-3	0.36	5	4.5±2.1	0.9	6	9.0±0.7
532	PASS-3	0.54	8	6.9±1.0	0.9	6	7.6±0.9
781	PASS-3	0.36	9	3.7±0.6	0.54	20	3.7±0.6
		Ethylene Premixed Flame Nascent (BC2)					
405	PASS-3	0.36	6	5.6±1.9	1.08	7	10.54±2.2
532	NOAA CRD-PAS	0.36	5	4.1±0.9	0.9	6	6.9±1.5
532	PASS-3	0.54	6	5.5±1.0	0.9	6	6.4 ± 1.2
781	PASS-3	0.36	9	2.3±0.5	0.54	14	2.8± 0.5

Table S5. Observed mean *MAC*s from the BC3+ ethylene flame.

λ (nm)	*MAC* (m^2 g^{-1}) $d_{p,VED}$ 50-70 nm	*MAC* (m^2 g^{-1}) $d_{p,VED}$ 70-130 nm	*MAC* (m^2 g^{-1}) $d_{p,VED}$ > 130 nm
405	8.2 ± 2.6	9.5 ± 1.9	9.9 ± 1.7
532	4.8 ± 0.80	6.2 ± 1.0	5.7 ± 0.90
630	2.9 ± 0.90	3.7 ± 0.5	4.0 ± 0.7

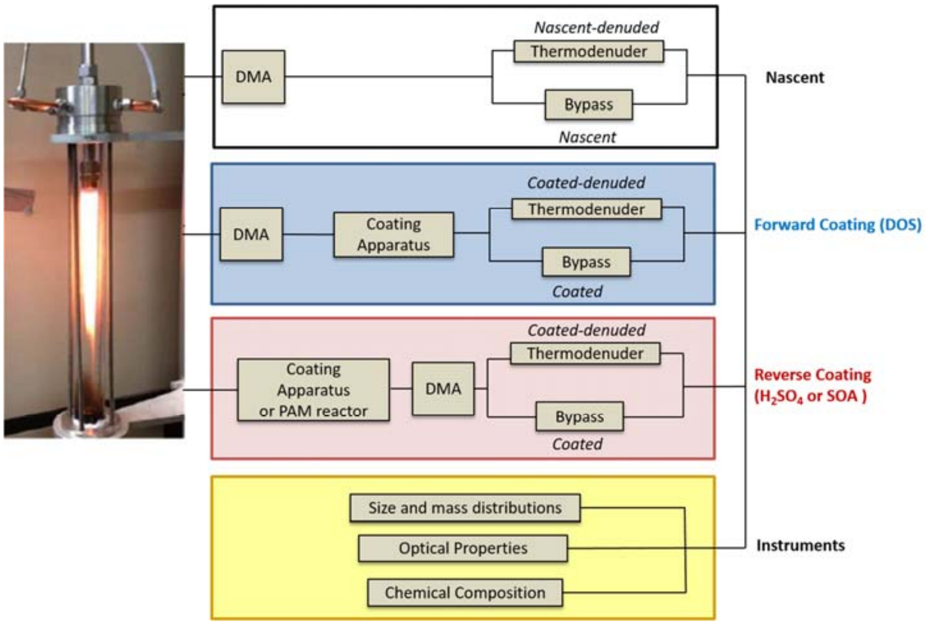

Figure S1. General experimental set-up for BC2, BC3, BC3+, and BC4, for the methane diffusion flame. Note that during BC4, particles were mass-selected with a CPMA, in addition to being size-selected.

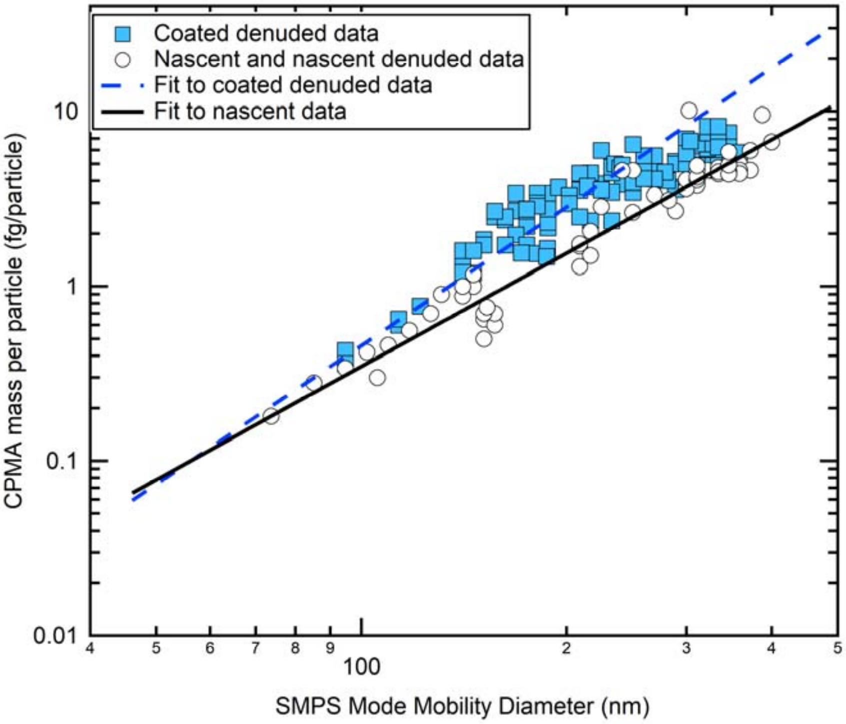

Figure S2. Observations and fits of CPMA mass per particle as a function of the SMPS mode number-weighted mobility diameter for methane diffusion flame soot particles. The blue squares show coated denuded observations and the dashed blue line is the power law fit to the coated-denuded data. The white circles are nascent observations and the black line is the power law fit to the nascent observations. Note that the fits to the coated-denuded data are for particles with mobility diameter < 260 nm since the large particles generally have thinner coatings and are therefore more fractal-like. The data were fit to a power law function (see eqn. 8 in the main text). For nascent soot, fit parameters C and $D_{f,m}$ were 1.70×10^{-5} and 2.12, respectively, and for coated-denuded soot, fit parameters C and $D_{f,m}$ were 2.44×10^{-6} and 2.64, respectively.

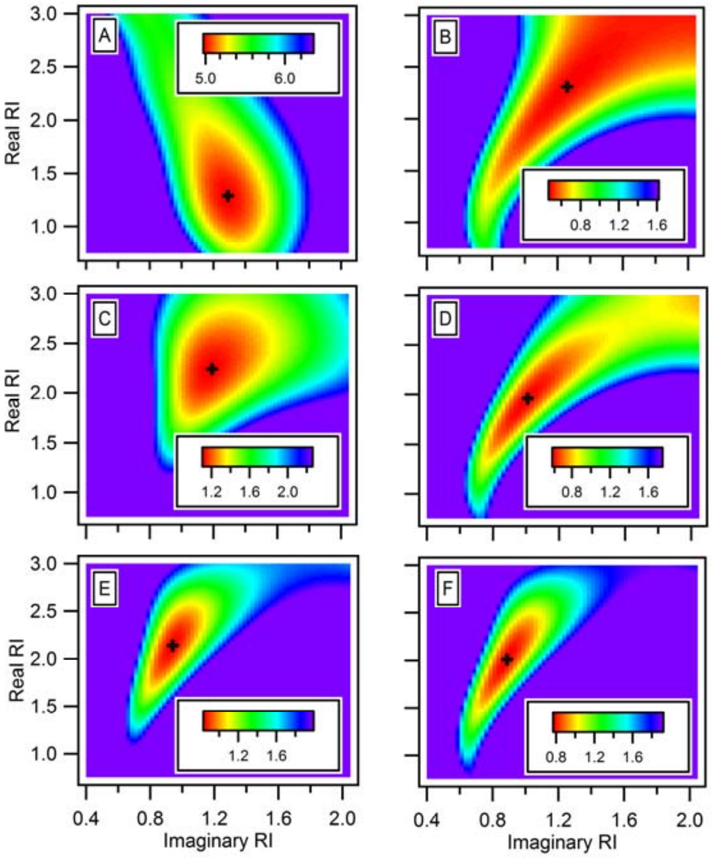

Figure S3. Image plots of the reduced χ^2 values of Mie Theory fits to absorption for all methane flame data. The colors represent the reduced χ^2 value at each effective refractive index. Each panel differentiates between different wavelengths. The column on the left is the fit over all size parameters and the column on the right corresponds to size parameter (x)<0.9. The minimum reduced χ^2 are shown as black crosses. Panels A and B correspond to λ = 405 nm data, panels C and D correspond to λ = 532 nm data, and panels E and F correspond to λ = 630 nm data. Purple on the image plots indicates the region beyond 1 standard deviation of the reduced χ^2 value (χ^2+1.11).

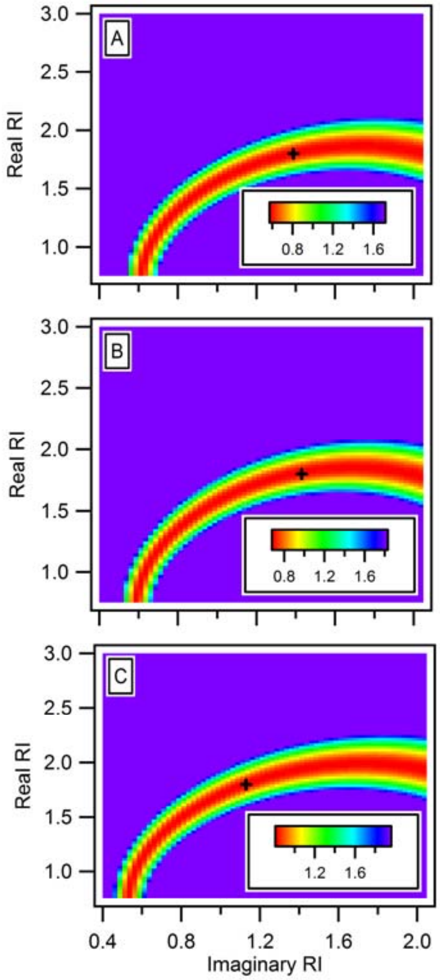

Figure S4. Same as Figure S3, except for RDG fits instead of Mie fits over all size parameters. Panel A, B, and C correspond to λ = 405 nm, 532 nm, and 630 nm data, respectively. Note that the crosses shown are not global minima, but selected to have *m* = 1.80. This is because there is no unique solution for the RDG fits.

Formatted: Font: Not Bold

Deleted: Figure S3

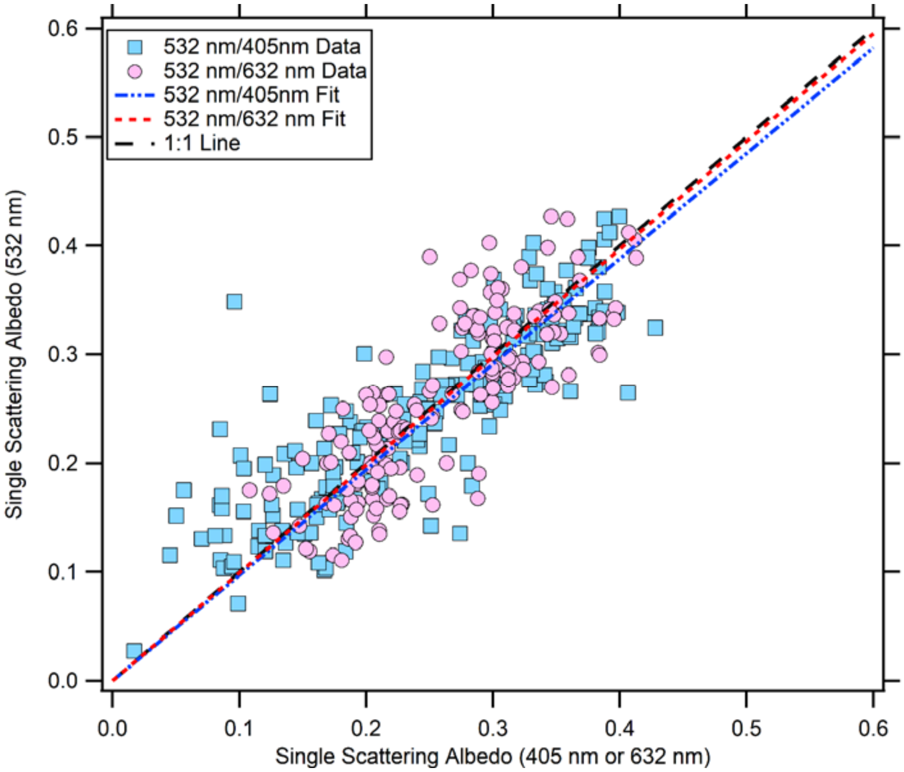

Figure S5. Comparison between observations of the single scattering albedo (*SSA*) at λ = 532 nm and at λ = 405 nm (blue squares) or at λ = 630 nm (pink circles) for the methane diffusion flame. The blue dashed line is a linear fit to the λ = 405 nm and 532 nm SSA pair, the red dashed line is the fit to the λ = 630 nm and 532 nm SSA pair. The black line is the 1:1 line. Note the generally good agreement between the *SSA*s between wavelengths. The best-fit slope was 0.97 for the λ = 405 nm/532 nm pair and 0.99 for the λ = 630 nm/532 nm pair.

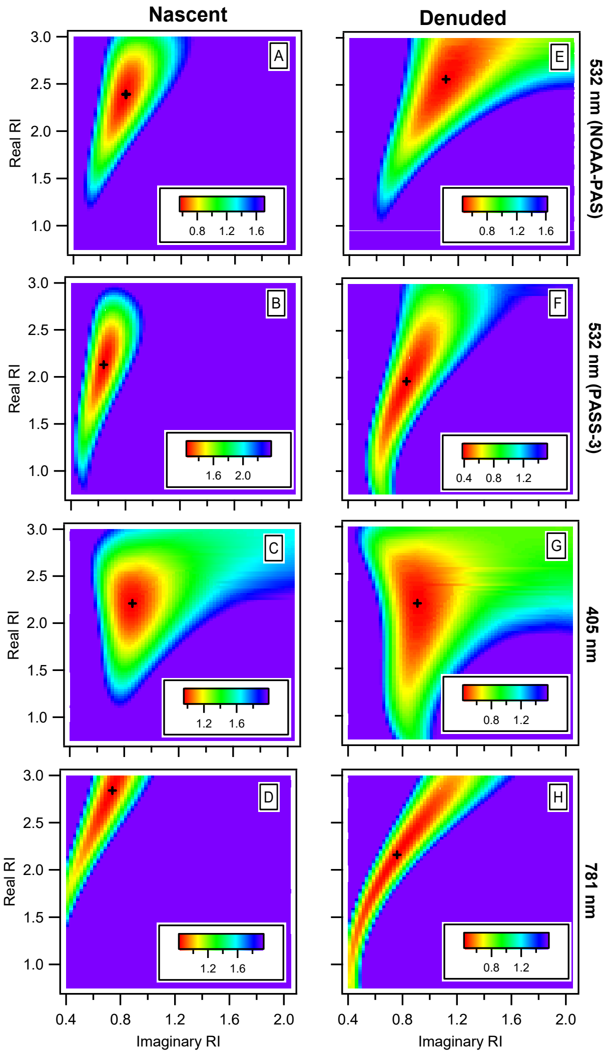

Figure S6. Image plots of the reduced χ^2 values of Mie Theory fits to absorption for all ethylene flame (20 cm sampling height) data from BC2. Colors indicate reduced χ^2 values, with the minima values shown as black crosses. Purple indicates the region beyond 1σ of the minimum reduced χ^2 value (χ^2+1.11). Each panel is for a particular wavelength and soot type (nascent vs. thermodenuded). The left column (A-D) is for nascent soot. The right column (E-H) is for denuded soot. Panels A and E are λ = 532 nm NOAA PAS data, panels B and F are λ = 532 nm PASS-3 data, panels C and G are λ = 405 nm PASS-3 data, and D and H are λ = 781 nm PASS-3 data.

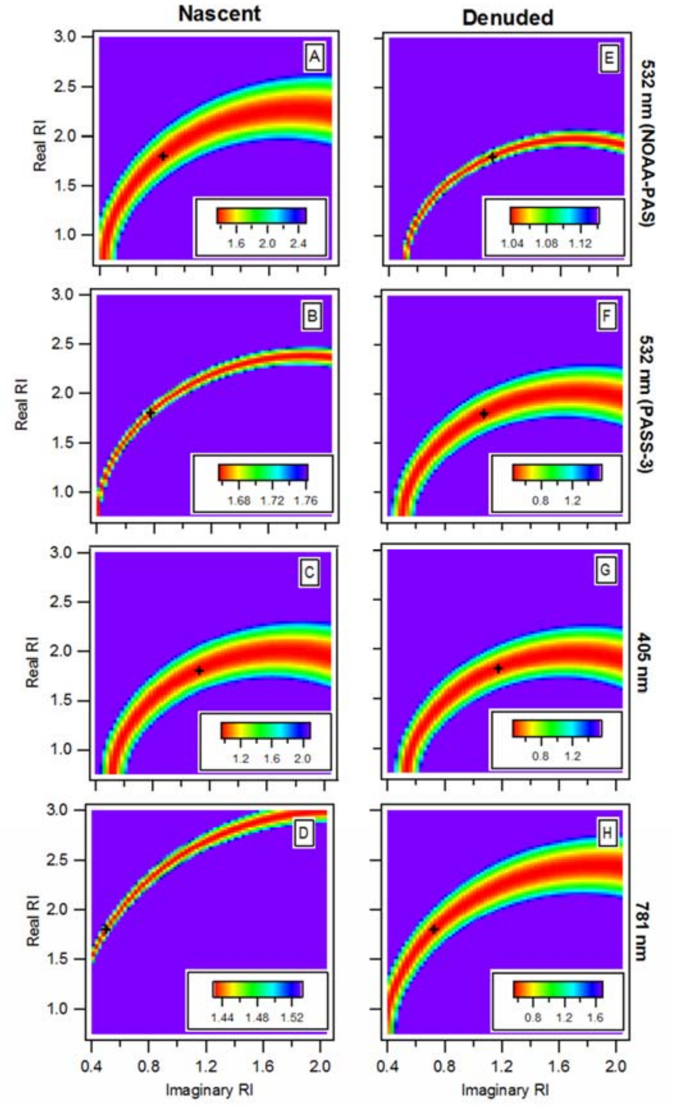

Figure S7. Same as Figure S6, except for RDG fits instead of Mie fits. Panel letters correspond to the same datasets as Figure S6. Note that the crosses shown are not global minima, but selected to have *m* = 1.80. This is because there is no unique solution for the RDG fits.

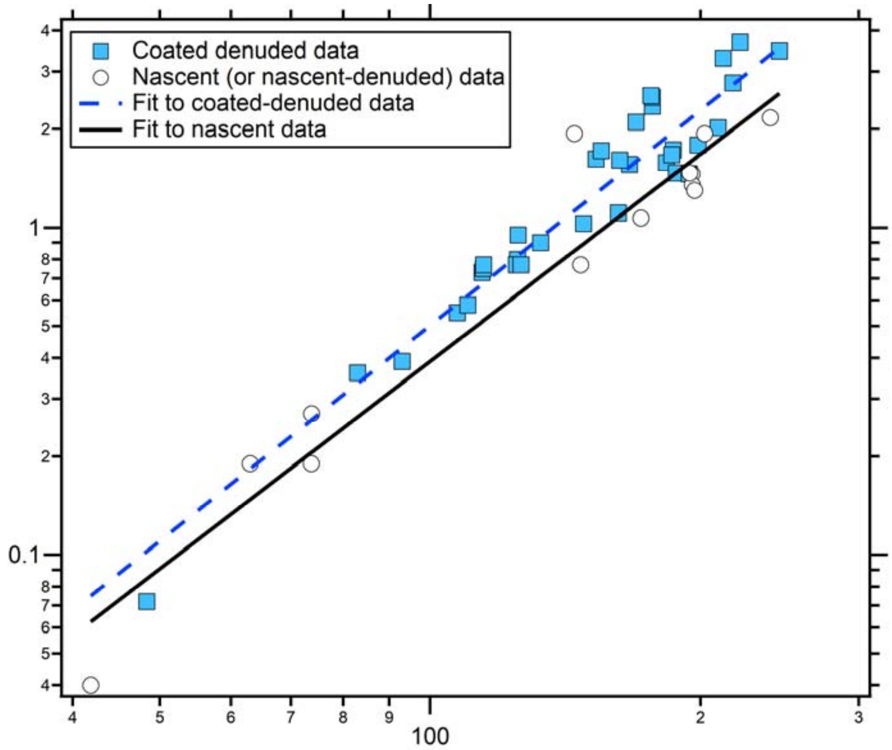

Figure S8. Fit of CPMA mass per particle as a function of the SMPS mode number-weighted mobility diameter for soot particles from the premixed ethylene flame from BC2, when the flame was sampled at 20 cm above the burner surface. The blue squares are coated denuded observations and the dashed blue line is the associated power-law fit. The white circles are nascent observations and the black line is the associated power-law fit. The data were fit to a power law function (see eqn. 8 in the main text). For nascent soot, fit parameters *C* and $D_{f,m}$ were 2.40 x 10^{-5} and 2.12, respectively, and for coated-denuded soot, fit parameters *C* and $D_{f,m}$ were 1.33 x 10^{-5} and 2.28, respectively.

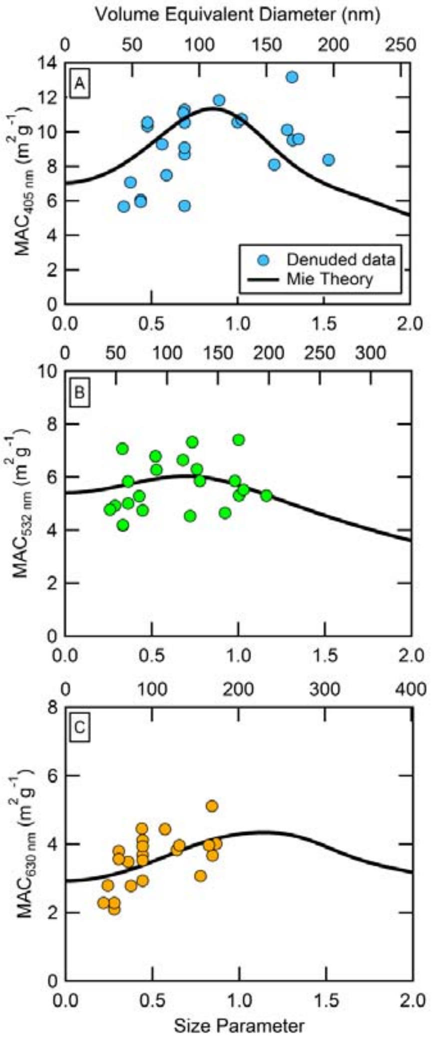

Figure S9. *MAC*s for ethylene soot sampled 5.1 cm above the burner surface as a function of size parameter (bottom) and volume equivalent diameter (top) for **(A)** λ =405 nm, **(B)** λ = 532 nm, and **(C)** λ = 630.

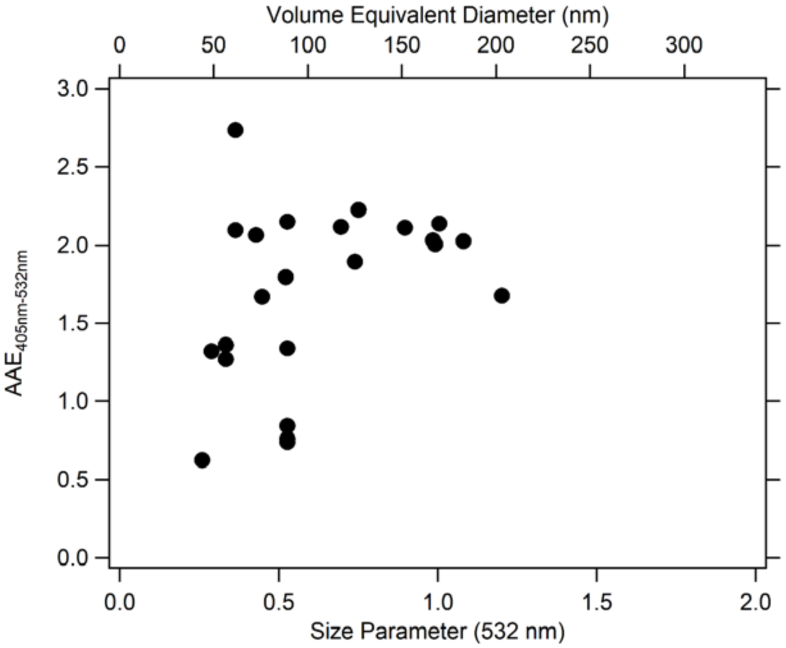

Figure S10. Absorption Ångström exponent (*AAE*) calculated using data measured at λ = 405 nm and λ = 532 nm as a function of size parameter (at λ = 532 nm) and volume equivalent diameter produced from the ethylene flame during BC3+.